H. Niewodniczański
INSTITUTE OF NUCLEAR PHYSICS,
Kraków, Poland.

REPORT No. 1620/PH

SMALL x PHYSICS *

Jan Kwieciński

Henryk Niewodniczański Institute of Nuclear Physics
Department of Theoretical Physics
ul. Radzikowskiego 152, 31-342 Kraków, Poland

* Lectures given at the 23nd Schladming Winter School: "Substructures of Matter as Revealed with Electroweak Probes", Schladming, Austria, 24th February - 5th March 1993.

Kraków 1993

WYDANO NAKŁADEM
INSTYTUTU FIZYKI JĄDROWEJ
IM. HENRYKA NIEWODNICZAŃSKIEGO
KRAKÓW, UL. RADZIKOWSKIEGO 152

Kopię kserograficzną, druk i oprawę wykonano w IFJ Kraków

Wydanie I zam. 37/93 Nakład 125 egz.

SMALL x PHYSICS *

J. Kwieciński

Department of Theoretical Physics, H. Niewodniczański Institute of Nuclear Physics, ul. Radzikowskiego 152, 31-342 Kraków, Poland.

Abstract.

The QCD expectations concerning the small x limit of parton distributions where x is the Bjorken scaling variable are reviewed. This includes discussion of the evolution equations in the small x region, the Lipatov equation which sums the leading powers of $\ln(1/x)$ and the shadowing effects. Phenomenological implications of the theoretical expectations for the deep inelastic lepton-hadron scattering in the small x region which will be accessible at the HERA ep collider are described. We give predictions for structure functions F_2 and F_L and discuss specific processes sensitive to the small x physics such as heavy quark production, deep inelastic diffraction and jet production in deep inelastic lepton scattering. A brief review of nuclear shadowing in the inelastic lepton nucleus scattering at small x is also presented.

---

* Lectures given at the 32nd Schladming Winter School: "Substructures of Matter as Revealed with Electroweak Probes"; Schladming, Austria, 24th February - 5th March 1993.

CONTENTS.

1. INTRODUCTION.

Small x physics is very interesting both theoretically as phenomenologically. We shall be primarily concerned with the deep-inelastic lepton-hadron scattering in the small x limit where x is the Bjorken scaling variable. The variable x is defined as :

$$x = \frac{Q^2}{2pq} \tag{1.1}$$

where

$$Q^2 = -q^2 \tag{1.2}$$

and p and q are the four momenta of a hadron and of the virtual photon respectively [1]. For large Q^2 we expect that the deep inelastic lepton-hadron scattering can be described within the QCD improved parton model [1-5]. The deep inelastic scattering at small x is then probing the parton distributions in a limit when the momentum fraction x carried by a parton is very small. QCD predicts several novel phenomena to occur in the small x limit of parton distributions such as the very strong increase of parton densities, parton screening effects possibly leading to parton saturation [6-11]. Understanding of parton distributions in this new regime is one of the most interesting and challenging theoretical problems in QCD. Moreover the HERA ep collider will be able to probe the very small x region for reasonably high values of Q^2 for the parton model ideas to be applicable [11-13]. It is therefore important to know whether various QCD expectations at small x can be tested experimentally.

The main aim of these lectures is to summarise the QCD expectations concerning the small x behaviour of parton distributions and to discuss their possible phenomenological implications for HERA. We shall also discuss nuclear shadowing in inelastic lepton-nucleus scattering at small x.

2. SMALL x LIMIT OF PARTON DISTRIBUTIONS IN PERTURBATIVE QCD.

2.1 Altarelli-Parisi evolution equations in the small x limit.

The Altarelli-Parisi evolution equations describe the evolution of quark and gluon densities with Q^2 [1-5,14]. In the leading $\log Q^2$ approximation LLQ^2 they have the following form:

$$Q^2\frac{\partial q_i(x,Q^2)}{\partial Q^2}=\frac{\alpha_s(Q^2)}{2\pi}[P_{qq}\otimes q_i+P_{qg}\otimes g]$$
$$Q^2\frac{\partial g(x,Q^2)}{\partial Q^2}=\frac{\alpha_s(Q^2)}{2\pi}[P_{gq}\otimes \Sigma+P_{gg}\otimes g] \qquad (2.1.1)$$

where

$$P_{ij}\otimes f=\int_x^1\frac{dx'}{x'}P_{ij}(\frac{x}{x'})f(x',Q^2) \qquad (2.1.2)$$

and

$$\Sigma(x,Q^2)=\sum_{i=1}^{N_f}[q_i(x,Q^2)+\bar{q}_i(x,Q^2)] \qquad (2.1.3)$$

The functions $g(x,Q^2)$ and $q_i(x,Q^2)$ and $\bar{q}_i(x,Q^2)$ are the gluon, quark and antiquark distributions where the index i denotes the quark flavour. $\alpha_s(Q^2)$ is the running QCD coupling [1-5] and N_f denotes the number of active flavours. The quark distributions $q_i(x,Q^2)$ are equal to the sum of the valence and sea quark distributions i.e.:

$$q_i(x,Q^2)=q_i^v(x,Q^2)+q_i^s(x,Q^2) \qquad (2.1.4)$$

and

$$q_i^s(x,Q^2)=\bar{q}_i(x,Q^2) \qquad (2.1.5)$$

The functions $P_{ij}(z)$ are the familiar splitting functions [1-5]. The valence quark distributions $q_i^v(x,Q^2)$ satisfy the following equation:

$$Q^2\frac{\partial q_i^v(x,Q^2)}{\partial Q^2}=\frac{\alpha_s(Q^2)}{2\pi}P_{qq}\otimes q_i^v \qquad (2.1.6)$$

The structure function $F_2(x,Q^2)$ of deep inelastic (charged) lepton scattering is related in the standard way to the quark and antiquark distributions:

$$F_2(x,Q^2)=\sum_{i=1}^{N_f}e_i^2x[q_i(x,Q^2)+\bar{q}_i(x,Q^2)] \qquad (2.1.7)$$

where e_i is the electric charge of the quark having a flavour i. Both the evolution equations as well as the relation (2.1.7) between the structure function F_2 and the quark distributions acquire additional higher order terms in $\alpha_s(Q^2)$ in the next-to-leading approximation (NLLQ2) [1-5].

In physical gauges the Altarelli-Parisi equations in the LLQ^2 approximation correspond to ladder diagrams with ordered longitudinal momenta and strongly ordered transverse momenta along the chain (see Fig. 1)

$$x < x_n < ..... < x_1 < 1$$

$$Q^2 >> \kappa^2 >> k_n^2 >> .....k_1^2 \tag{2.1.8}$$

In order to solve the evolution equations (2.1.1) and (2.1.6) one has to provide the input parametrisation of those distributions at some reference scale Q_0^2 which should be large enough for the QCD improved quark parton model to be applicable. The small x behaviour of the input parton distributions is usually obtained from Regge theory [1,9]:

$$xq_i^v(x,Q_0^2) \sim x^{1-\alpha_R} \tag{2.1.9}$$

$$xq_i^s(x,Q_0^2) \sim x^{1-\alpha_P}$$

$$xg(x,Q_0^2) \sim x^{1-\alpha_P} \tag{2.1.10}$$

where α_R and α_P denote the reggeon and pomeron intercepts respectively. Assuming that $\alpha_R \simeq 1/2$ and $\alpha_P \simeq 1$ we get the following behaviour for the valence quark, sea quark and gluon distributions at small x:

$$xq_i^v(x,Q_0^2) \sim x^{1/2} \tag{2.1.11}$$

$$xq_i^s(x,Q_0^2) \sim x^0$$

$$xg(x,Q_0^2) \sim x^0 \tag{2.1.12}$$

The $x^{1/2}$ type of behaviour of the valence quark distributions is stable against the QCD evolution generated by the eq. (2.1.6). The x^0 behaviour of the sea quark and gluon distributions is however unstable and for $Q^2 > Q_0^2$ the evolution equations (2.1.1) generate steeper behaviour i.e.:

$$xg(x,Q_0^2) \sim exp\{2[\eta(Q^2,Q_0^2)ln(1/x)]^{1/2}\} \tag{2.1.13}$$

with the similar behaviour for the sea quarks, where the function $\eta(Q^2,Q_0^2)$ is given by the following formula:

$$\eta(Q^2, Q_0^2) = \int_{Q_0^2}^{Q^2} \frac{dQ'^2}{Q'^2} \frac{3\alpha_s(Q'^2)}{\pi} \tag{2.1.14}$$

In (2.1.13) we have neglected a factor which is a slowly varying function of $\eta(Q^2, Q_0^2)$ $ln(1/x)$. The gluon and sea quark distributions (multiplied by x) are therefore found to grow faster than any power of $ln(1/x)$ in the small x limit.

This growth is generated by gluon exchange along the chain in Fig. 1 and comes from the fact that the splitting function $P_{gg}(z)$ is singular in the small z limit i.e.:

$$P_{gg}(z) \simeq \frac{6}{z} \tag{2.1.15}$$

The configuration $z << 1$ at each vertex corresponds to strongly ordered longitudinal momenta.

The approximation in which both the longitudinal and transverse momenta are strongly ordered and in which only the gluon exchange is retained along the chain with the singular part of the splitting function $P_{gg}(z)$ is called the double logarithmic approximation (DL). This approximation generates terms containing the leading powers of $\eta(Q^2, Q_0^2)ln(1/x)$. For large magnitude of this quantity those terms sum up to the expression given by the eq.(2.1.13).

When discussing the small x limit of parton distributions it is often convenient to use the moments of those distributions since the small x behaviour of parton distributions is controlled by the singularities of their moments in the moment index plane. The moment $g_n(Q^2)$ of the gluon distribution $g(x, Q^2)$ is defined as

$$g_n(Q^2) = \int_0^1 dx x^{n-1} g(x, Q^2) \tag{2.1.16}$$

and similarly for other parton distributions. The gluon distribution $g(x, Q^2)$ is related to the moments $g_n(Q^2)$ through the inverse Mellin transform:

$$g(x, Q^2) = \frac{1}{2\pi i} \int_{c-i\infty}^{c+i\infty} dn x^{-n} g_n(Q^2) \tag{2.1.17}$$

where the integration contour is located to the right of the singularities of the moment $g_n(Q^2)$ in the n plane. It is therefore clear from the eq. (2.1.17) that the (leading) small x behaviour of the gluon distributions is controlled by the leading (i.e. rightmost) singularity of $g_n(Q^2)$ in the n plane.

The evolution equations for moments can be solved in a closed form [1-5] and if we keep only the splitting function P_{gg} in the eq. (2.1.1) which is most relevant at small x this solution is:

$$g_n(Q^2) = g_n(Q_0^2) exp[\gamma_{gg}(n)\eta(Q^2, Q_0^2)] \tag{2.1.18}$$

where

$$\gamma_{gg}(n) = \frac{1}{6}\int_0^1 dz z^{n-1} P_{gg}(z) \tag{2.1.19}$$

and where $g_n(Q_0^2)$ is the moment of the starting distribution. If we keep only the singular term $6/z$ in P_{gg} (i.e. if we restrict ourselves to the double logarithmic approximation) then $\gamma_{gg}(n)$ is equal to

$$\gamma_{gg}^{DL}(n) = \frac{1}{(n-1)} \tag{2.1.20}$$

It follows from eqs.(2.1.18) and (2.1.20) that the moment $g_n(Q^2)$ has an essential singularity at $n = 1$. This is the leading singularity if the starting distribution has the behaviour (2.1.12) and it generates the small x behaviour given by the formula (2.1.13).

The solution of the evolution equations for the moments $q_{in}^v(Q^2)$ of the valence quark distributions is:

$$q_{in}^v(Q^2) = q_{in}^v(Q_0^2) exp[\gamma_{qq}(n)\eta(Q^2, Q_0^2)] \tag{2.1.21}$$

where

$$\gamma_{qq}(n) = \frac{1}{6}\int_0^1 dz z^{n-1} P_{qq}(z) \tag{2.1.22}$$

and the leading pole of the function $\gamma_{qq}(n)$ is at $n = 0$ [1,3-5]. The moment $q_{in}^v(Q_0^2)$ of the starting valence quark distribution will have a pole at $n = 1/2$ if this distribution has its small x behaviour given be the eq.(2.1.11). This pole will remain the leading singularity of the moment $q_{in}^v(Q^2)$ and in consequence the small x behaviour (2.1.11) of the valence quark distributions will remain unchanged by the QCD evolution.

The fact that the "x^0" behaviour of gluon and sea quark distributions is unstable against the QCD evolution suggests that the pomeron in QCD may be more complicated than just a simple Regge pole of intercept equal to 1. Moreover it should be realised that the LLQ^2 or DL approximations are incomplete in the small x limit. The LLQ^2 approximation sums by definition only those terms in the perturbative expansion which contain the leading powers of $ln(Q^2)$ at each order of the perturbative expansion. In the small x limit however we should sum at least those terms which contain the leading powers of $ln(1/x)$ and retain the full Q^2 dependence i.e. to consider the leading $\log(1/x)$ ($LL1/x$) approximation. This approximation leads to the Lipatov equation which will be described in the next Section.

2.2 The leading log(1/x) approximation and the Lipatov equation.

The leading $\log(1/x)$ approximation corresponds by definition to the sum of those terms in the perturbative expansion which contain the maximal powers of $ln(1/x)$ at each order of the perturbative expansion. The basic quantity in this approximation is the unintegrated gluon distribution $f(x,k^2)$ defined as:

$$f(x,k^2) = Q^2 \frac{\partial x g(x,Q^2)}{\partial Q^2}|_{Q^2=k^2} \tag{2.2.1}$$

where $g(x,Q^2)$ is the gluon distribution in a hadron. In the LL$1/x$ approximation the unintegrated gluon distribution satisfies the following equation [15-22]:

$$-\ x\frac{\partial f(x,k^2)}{\partial x} = \frac{3\alpha_s(k^2)}{\pi}k^2 \int_{k_0^2}^{\infty} \frac{dk'^2}{k'^2}\{\frac{f(x,k'^2)-f(x,k^2)}{|k'^2-k^2|} + \frac{f(x,k^2)}{[4k'^4+k^4]^{1/2}}\}$$

$$\equiv K_L \otimes f \tag{2.2.2}$$

This equation is called in the literature the Balitzkij-Fadin-Kuraev-Lipatov equation or, in short, the Lipatov equation. It corresponds again to the sum of ladder diagrams (see Fig. 2) but unlike the LLQ^2 approximation the transverse momenta of the gluons are not ordered. The kernel K_L of the eq.(2.2.2) contains both the real gluon emission terms as well as the virtual corrections. The former correspond to terms proportional to $f(x,k'^2)$ while the latter to terms proportional to $f(x,k^2)$ in the rhs. of the eq.(2.2.2). The virtual corrections correspond to the "gluon reggeisation"[6,15-18] (or to the "non-Sudakov" form factor [20-22]) The variable(s) $k^2(k'^2)$ correspond to the transverse momenta of the gluons. The parameter k_0^2 is the infrared cut-off which is necessary if the running coupling constant effects are taken into account. (Strictly speaking, within the genuine LL$1/x$ approximation, the QCD coupling α_s should be set to be k^2 independent.)

When the running coupling effects are neglected (i.e. when one sets $\alpha_s(k^2) = \bar{\alpha}_s$) and when $k_0^2 = 0$ then the equation (2.2.2) can be solved analytically. To this aim it is convenient to introduce the moment $f_n(k^2)$ of the function $f(x,k^2)$:

$$f_n(k^2) = \int_0^1 dx x^{n-2} f(x,k^2) \tag{2.2.3}$$

which satisfies the following integral equation:

$$f_n(k^2) = \frac{f_0(k^2)}{(n-1)} + \frac{3\bar{\alpha}_s}{\pi(n-1)} k^2 \int_0^\infty \frac{dk'^2}{k'^2} \{ \frac{f_n(k'^2) - f_n(k^2)}{|k'^2 - k^2|} + \frac{f_n(k^2)}{[4k'^4 + k^4]^{1/2}} \} \quad (2.2.4)$$

This equation can be solved by taking the Melin transform $\tilde{f}_n(r)$ of $f_n(k^2)$

$$\tilde{f}_n(r) = \int_0^\infty dk^2 (k^2)^{-r-1} f_n(k^2) \quad (2.2.5)$$

which gives:

$$\tilde{f}_n(r) = \frac{\tilde{f}_0(r)}{n - 1 - \frac{3\bar{\alpha}_s}{\pi}\tilde{K}(r)} \quad (2.2.6)$$

where $\tilde{K}(r)$ is the Mellin transform of the kernel of the integral equation (2.2.4), that is [6,16,17]

$$\tilde{K}(r) = -[\Psi(r) + \Psi(1-r) - 2\Psi(1)] \quad (2.2.7)$$

where $\Psi(z)$ is the logarithmic derivative of the Euler gamma function: $\Psi(z) \equiv \Gamma'(z)/\Gamma(z)$ The function $\tilde{f}_0(r)$ is the Mellin transform of the driving term $f_0(k^2)$. The moment $f_n(k^2)$ is given by the inverse Mellin transform

$$f_n(k^2) = \frac{1}{2\pi i} \int_{1/2-i\infty}^{1/2+i\infty} dr (k^2)^r \frac{\tilde{f}_0(r)}{n - 1 - \frac{3\bar{\alpha}_s}{\pi}\tilde{K}(r)} \quad (2.2.8)$$

The integrand in (2.2.8) has poles at the zeros of its denominator. They define the anomalous dimensions in the LL($1/x$) approximation [23]. Note that for $r = 1/2$ the two poles pinch the integration contour in (2.2.8) leading to the (branch point) singularity in the n plane at $n = 1 + \lambda$ where

$$\lambda = \frac{3\alpha_s}{\pi}\tilde{K}(1/2) \equiv \frac{12ln(2)}{\pi}\bar{\alpha}_s \quad (2.2.9)$$

The leading small x behaviour is then found to be given by the following formula:

$$f(x, k^2) \sim const(k^2)^{1/2} \frac{x^{-\lambda}}{[ln(1/x)]^{1/2}} [1 + O(1/ln(1/x)] \quad (2.2.10)$$

The parameter λ is equal to the maximal eigenvalue of the kernel K_L. The relatively unimportant factor $[ln(1/x)]^{-1/2}$ in the eq.(2.2.10) comes from the fact that for the fixed coupling $\bar{\alpha}_s$ the eigenvalue spectrum of the kernel K_L is continuous. If the running coupling effects are included in the Lipatov equation as displayed explicitly in the eq.(2.2.2)) then the eigenvalue spectrum of K_L becomes discrete. The leading small x behaviour is then:

$$f(x,k^2) \simeq x^{-\bar{\lambda}} \tag{2.2.11}$$

The maximal eigenvalue $\bar{\lambda}$ has to be now calculated numerically. It has been found to be dependent upon the infrared cut-off k_0^2 [24-28].

We found in this way that the gluon distributions in the LL1/x approximation (multiplied by x) grow as the negative power of x in the small x limit. It should be noted that the exponent λ can have potentially large magnitude $\simeq 1/2$ or so.

This singular behaviour cannot hold forever and for sufficiently small values of x it has to be tamed by the screening corrections which will be described in the next Section.

2.3 Parton screening.

We showed in the previous Section that the gluon distributions (multipled by x) i.e. the functions $xg(x,Q^2)$ can grow indefinitely in the small x limit. The gluon distribution $g(x,Q^2)$ is equal by definition to the number density of gluons having transverse size $\sim 1/Q$ and carrying the fraction x of the hadron momentum in the infinite momentum frame. The quantity $xg(x,Q^2)$ is then equal to the number of those gluons within a bin $\Delta x \simeq x$ or eqivalently to the number of gluons per unit rapidity $ln(1/x)$. The transverse area $\tilde{S}(x,Q^2)$ occupied by those gluons is then given by the following formula:

$$\tilde{S}(x,Q^2) = xg(x,Q^2)\tilde{S}_g(Q^2) \tag{2.3.1}$$

where $\tilde{S}_g(Q^2)$ is the transverse area of a single gluon. Let us assume that it is equal to the (total) cross-section corresponding to the interaction of the hard probe gluon of virtuality Q^2 with a gluon in a hadron i.e.:

$$\tilde{S}_g(Q^2) = const\frac{\alpha_s(Q^2)}{Q^2} \tag{2.3.2}$$

The total area occupied by the small x gluons is then given by:

$$\tilde{S}(x,Q^2) = const\ xg(x,Q^2)\frac{\alpha_s(Q^2)}{Q^2} \tag{2.3.3}$$

This formula describes at the same time the cross-section corresponding to the interaction of the probe with a hadron within a QCD improved parton model. We showed in the preceeding Sections that the quantity $xg(x,Q^2)$ can grow indefinitely with decreasing x. For sufficiently small value of x the transverse area occupied by the small x gluons can, for fixed Q^2, become comparable to the transverse area of a

hadron $S_H = \pi R_H^2$ where R_H is the hadronic radius. When this happens (and in fact before this happens), the gluons can no longer be treated as free partons. They begin to screen each other and interact. This interaction leads to screening (or shadowing) effects. The main effect of shadowing is to tame the indefinite increase of parton distributions. One finds instead that at the sufficiently small values of x and/or Q^2 the gluon distributions approach the so-called saturation limit $xg_{sat}(x,Q^2)$ [6]

$$xg_{sat}(x,Q^2) = \frac{const}{\alpha_s(Q^2)} R_H^2 Q^2 \tag{2.3.4}$$

In some models [29] the saturation limit contains some remnant weak x dependence. The most dramatic effect is the linear scaling violation exhibited by $xg_{sat}(x,Q^2)$.

If one assumes that the gluons are not distributed uniformly within a hadron but are concentrated around the "hot-spots" [30,31] having their radius $R_{h.s.}$ much smaller than the hadronic radius R_H then the shadowing effects are expected to be stronger. The saturation limit $xg_{sat}(x,Q^2)$ is then controlled by the radius $R_{h.s.}$ and not by R_H.

The shadowing effects modify the evolution equations as well as the Lipatov equation by the non-linear terms. Thus the Lipatov equation with shadowing has the following form [6,25]:

$$-x\frac{\partial f(x,k^2)}{\partial x} = \frac{3\alpha_s(k^2)}{\pi} k^2 \int_{k_0^2}^{\infty} \frac{dk'^2}{k'^2} \{ \frac{f(x,k'^2) - f(x,k^2)}{|k'^2 - k^2|} + \frac{f(x,k^2)}{[4k'^4 + k^4]^{1/2}} \}$$

$$- \frac{81\alpha_s^2(k^2)}{16R^2k^2} [xg(x,k^2)]^2 \tag{2.3.5}$$

This equation is called in the literature the Gribov, Levin, Ryskin (GLR) equation.

The second term in the right hand side of the eq.(2.3.5) which is quadratic in the gluon distributions describes the shadowing effects . They correspond to the diagrams shown in Fig. 3. The parameter R describes the size of the region within which the gluons are concentrated. It arises from the integration over the 4-momentum δ flowing along the gluon ladders in Fig. 3. Specifically R comes from the integration over the transverse components of δ,

$$\frac{1}{R^2} \sim \int d\delta_T^2 [F(-\delta_T^2)]^2 \tag{2.3.6}$$

and its value depends on exactly how the gluon ladders couple to the hadron. If the ladders couple to different partons (see Fig. 4a), then the form factor F is characterised by the hadronic radius, that is $R \sim 5GeV^{-1}$. If we include a possibility that the ladders couple to the same constituent of the hadron (Fig. 4b) then it is appropriate to take R to be the radius of a valence quark, that is $R \sim 2GeV^{-1}$. It is in the latter case when we speak about "hot-spots" [30,31].

The diagrams describing the shadowing effects in quark distributions which will be introduced in the next Section are shown in Figs. 5a and 5b.

Analysis of the equation (2.3.5) permits to study the onset of the singular $x^{-\lambda}$ type of behaviour generated by the Lipatov kernel and a simultaneous taming of this behaviour by the non-linear shadowing term. This analysis has been performed in [25,32] where the eq. (2.3.5) was solved by evolving in x downwards starting from the phenomenological boundary conditions at $x = x_0 = 10^{-2}$. The gluon distributions which come out from this analysis are presented in Figs.6a and 6b. It may be seen that in the case when the shadowing term is neglected the $x^{-\lambda}$ behaviour emerges very clearly. It may also be seen that the shadowing corrections are rather small in the region of moderately small values of x ($x > 10^{-4}$ or so) at least for $R = 5GeV^{-1}$.

We can quantify the role of the shadowing effects introducing the parameter $W'(x,Q^2)$ equal to the ratio of the quadratic term to the linear term in the rhs of the eq.(2.3.5). One may consider three regions in the (x,Q^2) plane depending upon the magnitude of $W'(x,Q^2)$.

(i) In the region where $W'(x,Q^2) << \alpha_s(Q^2)$ the shadowing is negligible.

(ii) For $W'(x,Q^2) \simeq \alpha_s(Q^2)$ the shadowing becomes significant. It is expected to be described by the "leading" term which is quadratic in the gluon distribution as in the eq. (2.3.5).

(iii) In the region where $W'(x,Q^2) >> \alpha_s(Q^2)$ (i.e. $W'(x,Q^2) = O(1)$) the "leading" shadowing approximation may become inadequate. This is the very interesting region characterised by high density of weakly interacting partons (we assume that $\alpha_s(Q^2)$ is small) [29]. In this region the parton distributions are expected to be close to their saturation limit.

The parameter $W'(x,Q^2)$ is shown in Figs. 6c and 6d. It turns out that in the region of x and Q^2 which may be relevant for HERA its magnitude is still relatively small at least for $R \sim 5GeV^{-1}$.

More insight into the structure of the non-linear equation (2.3.5) can be obtained from its approximate form in which the linear part corresponds to the double logaritmic approximation (see Section 2.1). This approximation leads to the following equation [6,33-36]:

$$-Q^2 x\frac{\partial^2 xg(x,Q^2)}{\partial Q^2 \partial x} = \frac{3\alpha_s(Q^2)}{\pi} xg(x,Q^2) - \frac{81\alpha_s(Q^2)^2}{16R^2Q^2}[xg(x,Q^2)]^2 \qquad (2.3.7)$$

One may study this equation using the so-called semiclassical approximmation in which one neglects the second order derivatives of the function $S(x,Q^2) = ln[xg(x,Q^2)]$ [6,35,36]. As the result one obtains the following non-linear partial differential equation containing only first order derivatives of $S(x,Q^2)$:

$$- Q^2 x \frac{\partial S(x,Q^2)}{\partial Q^2} \frac{\partial S(x,Q^2)}{\partial x} = \frac{3\alpha_s(Q^2)}{\pi} - \frac{81\alpha_s(Q^2)^2}{16R^2Q^2} exp[S(x,Q^2)] \qquad (2.3.8)$$

which may be solved using the method of characteristics [34-36]. It turns out that the characteristic lines can be divided into two classes on either side of the critical line $y_c(\xi)$ which itself is also a solution of the characteristic equations [here $\xi = ln[ln(Q^2/\Lambda^2)$ where Λ is the QCD scale parameter and $y = ln(1/x)$]. Below the critical line we have $W'(x,Q^2) << \alpha_s(Q^2)$ while on the critical line $W'(x,Q^2) = O[\alpha_s(Q^2)]$. In the "high density" region above the critical line the characteristic curves approach infinity for a given value $\xi = \tilde{\xi}$ depending upon the boundary conditions and the parameters defining the shadowing term. The limit $y(\xi) \to \infty$ for $\xi \to \tilde{\xi}$ corresponds to $W'(x,Q^2) \to 1$ and $xg(x,Q^2) \to xg_{sat}(x,Q^2)$. The saturation limit in this case corresponds to the gluon distribution for which the right hand side of the eq. (2.3.7) vanishes i.e.:

$$xg_{sat}(x,Q^2) = \frac{16}{27\pi\alpha_s(Q^2)} R^2Q^2 \qquad (2.3.9)$$

The pattern of the characteristic lines described above is displayed in Fig.7

It turns out however that the parameter $W'(x,Q^2)$ obtained from the exact solution of the eq. (2.3.5) can have acceptable small values in regions above the semiclassical critical line. This in particular takes place in the region of (x,Q^2) which may be accessible at HERA. The semiclassical critical line should not therefore be regarded in general as the genuine boundary between the regions of low and high gluon densities.

It is also possible to formulate the semiclassical approximation of the original equation (2.3.5) [25,37].

3. SMALL x PHYSICS IN DEEP INELASTIC LEPTON-HADRON SCATTERING.

3.1 The QCD predictions for the deep-inelastic structure functions at small x.

In the previous Sections we have described the QCD expectations concerning the small x behaviour of parton distributions. Our discussion focussed entirely on gluon distributions which dominate at small x. The singular small x behaviour, shadowing effects etc. should also manifest themselves in the sea quark distributions which at small x are predominantly driven by the gluons. It is the sea quark distributions which dominate in the structure function F_2 at small x. The longitudinal structure function $F_L(x,Q^2)$ is at small x also dominated by the gluons and in perturbative QCD one gets the following formula for $F_L(x,Q^2)$ [1]:

$$F_L(x,Q^2) = \frac{\alpha_s(Q^2)}{\pi}\{\int_x^1 \frac{dy}{y}(\frac{x}{y})^2 F_2(y,Q^2)$$

$$+2\sum e_q^2 \int_x^1 \frac{dy}{y}(\frac{x}{y})^2(1-\frac{x}{y})yg(y,Q^2)\} \qquad (3.1.1)$$

We shall now briefly discuss how the QCD expectations can be (approximately) incorporated within the phenomenological analysis of deep inelastic lepton -hadron scattering and of related processes based on the Altarelli-Parisi evolution equations.

In order to implement phenomenologically the singular $x^{-\lambda}$ type behaviour (with $\lambda \simeq 1/2$) and shadowing effects one proceeds as follows [38]:

(i)The singular behaviour and screening effects are incorporated in the parametrisation of the input distributions at the reference scale Q_0^2 which is usually set equal $4GeV^2$.

The unshadowed gluon distribution xg^u is assumed to take the form:

$$xg^u(x,Q_0^2) = C(x)x^{-\lambda} \qquad (3.1.2)$$

where $\lambda \simeq 1/2$ and where the function $C(x)$ is non-singular at $x = 0$. The same parametrisation is assumed to hold for the unshadowed sea quark distributions (but, of course, with the different function $C(x)$). The shadowed (input) distribution are modified as below:

$$xg(x,Q_0^2) = \frac{xg^u(x,Q_0^2)}{\{1+\theta(x_0-x)[xg^u(x,Q_0^2)-xg^u(x_0,Q_0^2)]/xg_{sat}(x,Q_0^2)\}} \qquad (3.1.3)$$

$$xq_i^s(x,Q_0^2) = xq_i^{s(u)}(x,Q_0^2)\frac{xg(x,Q_0^2)}{xg^u(x,Q_0^2)} \tag{3.1.4}$$

where $xg_{sat}(x,Q_0^2)$ is defined by the eq.(2.3.9). The shadowing effects are in this way switched on only for $x < x_0$ where x_0 is usually set equal 10^{-2}.

(ii) The input parton distributions are then evolved in Q^2 using the QCD evolution equations with the non-linear terms describing shadowing effects both for gluons as well as for the sea quarks. Those evolution equations have the following form [33]:

$$Q^2\frac{\partial xg(x,Q^2)}{\partial Q^2} = \frac{\alpha_s(Q^2)}{2\pi}x[P_{gq}\otimes\Sigma + P_{gg}\otimes g]$$

$$-\frac{81\alpha_s^2(Q^2)}{16R^2Q^2}\theta(x_0-x)\int_x^{x_0}\frac{dx'}{x'}[x'g(x',Q^2)]^2 \tag{3.1.5a}$$

$$Q^2\frac{\partial xq_i(x,Q^2)}{\partial Q^2} = \frac{\alpha_s(Q^2)}{2\pi}x[P_{qq}\otimes q_i + P_{qg}\otimes g]$$

$$-\frac{27\alpha_s^2(Q^2)}{160R^2Q^2}[xg(x,Q^2)]^2 + \frac{\alpha_s(Q^2)}{\pi Q^2}\theta(x_0-x)\int_x^{x_0}\frac{dx'}{x'}\frac{x}{x'}\gamma(\frac{x}{x'})x'G_H(x',Q^2) \tag{3.1.5b}$$

$$Q^2\frac{\partial xG_H(x,Q^2)}{\partial Q^2} = -\frac{81\alpha_s^2(Q^2)}{16R^2Q^2}\theta(x_0-x)\int_x^{x_0}\frac{dx'}{x'}[x'g(x',Q^2)]^2 \tag{3.1.5c}$$

where

$$\gamma(z) = -2z + 15z^2 - 30z^3 + 18z^4 \tag{3.1.6}$$

(iii) In the region of "large" x ($x > 10^{-2}$ or so) the parton distributions are constrained phenomenologically by the available data on deep inelastic lepton-hadron scattering and on other hard processes.

In Fig. 8 we show the recent results of this analysis for the structure function $F_2(x,Q^2)$ [39]. This Figure shows predictions concerning the behaviour of the structure function $F_2(x,Q^2)$ based on two sets of parton distributions, D_- and D_0 which respectively include and omit an $x^{-1/2}$ factor in the input distributions. Both sets describe the existing "large" x ($x > 0.05$ or so) data equally well. In the D_- case we also show results with and without shadowing corrections for two values of the radius parameter R i.e. for $R = 5GeV^{-1}$ (weak shadowing) and for $R = 2GeV^{-1}$ (strong shadowing motivated by the "hot spots" scenario) respectively. It can be seen that the shadowing effects are expected to be small in the small x region relevant for HERA (i.e. for $x \sim 10^{-3}$).

A missing ingredient in the procedure described above is any constraint on the size of the Lipatov component i.e. on that part of the gluon and sea quark distributions which has the $x^{-\lambda}$ behaviour with $\lambda \simeq 1/2$. The gluon distribution has not been required to satisfy the Lipatov equation (see Sec. 2.2); simply the $x^{-1/2}$ behaviour has been imposed on the input distribution at the reference scale $Q^2 = Q_0^2$, and also on the sea quark distributions which are themselves driven by the gluons.

We shall now discuss more quantitative predictions for the behaviour of the structure functions $F_2(x,Q^2)$ and $F_L(x,Q^2)$ at small x which will be directly based on the Lipatov equation [40]. The relevant diagrams are shown in Fig. 9 and the contribution to the (transverse and longitudinal) deep inelastic structure functions can be written in the following factorizable form [41-43]:

$$F_{T,L}(x,Q^2) = \int_x^1 \frac{dx'}{x'} \int \frac{dk_T^2}{k_T^4} f(\frac{x}{x'}, k_T^2) F_{T,L}^{(0)}(x', k_T^2, Q^2) \qquad (3.1.7)$$

where x/x' is the longitudinal momentum fraction carried by the gluon which couples to the $q\bar{q}$ pair. The functions $F_{T,L}^{(0)}$ denote the quark box (and crossed box) approximation to the photon-gluon subprocess shown in the upper part of the diagrams shown in Fig. 9. In other words $F_{T,L}^{(0)}$, or to be dimensionally correct $F_{T,L}^{(0)}/k_T^2$, may be regarded as the structure functions of a gluon of approximate virtuality k_T^2. The function $f(x/x', k_T^2)$ is the unintegrated gluon density corresponding to the sum of ladder diagrams in the lower part of the diagrams shown in Fig. 9. In the leading log $(1/x)$ approximation or, to be precise in the leading $\log(x'/x)$ approximation, the function f is given as the solution of the Lipatov equation (see Sections 2.2 and 2.3).

It may be instructive to see how the general factorizable form (3.1.7) reduces to the Altarelli-Parisi evolution of $q\bar{q}$ radiation from a gluon. In the Altarelli-Parisi treatment in the leading $\log Q^2$ approximation the integrations over the transverse momenta are dominated by the contributions from the strongly ordered configuration $k_T^2 << \kappa_T^2 << Q^2$ (see Sec. 2.1). In this limit there is no contribution to F_L and so we need only consider the structure function $F_2(x,Q^2)$. If we keep only the strongly ordered contribution and we recall that x' is the momentum fraction of the gluon carried by the quark (or antiquark) which is struck by the photon, then F_2^0 which is equal to F_T^0 of (3.1.7) in the LLQ^2 approximation is given by

$$F_2^{(0)}(x', k_T^2, Q^2) = \int_{k_T^2}^{Q^2} \frac{d\kappa_T^2}{\kappa_T^2} 2 \sum_q e_q^2 \frac{\alpha_s(\kappa_T^2)}{2\pi} x' P_{qg}(x') \qquad (3.1.8)$$

where $P_{qg}(x')$ is the Altarelli-Parisi splitting function. Thus (3.6) becomes

$$F_2(x,Q^2) = \int_x^1 dx' \int^{Q^2} \frac{d\kappa_T^2}{\kappa_T^2} \int^{\kappa_T^2} \frac{dk_T^2}{k_T^2} f(\frac{x}{x'}, k_T^2) 2 \sum_q e_q^2 \frac{\alpha_s(\kappa_T^2)}{2\pi} P_{qg}(x') \qquad (3.1.9)$$

and hence, using (2.2.1), we have

$$Q^2 \frac{\partial F_2(x,Q^2)}{\partial Q^2} = 2 \sum_q e_q^2 \frac{\alpha_s(Q^2)}{2\pi} \int_x^1 dx' P_{qg}(x') \frac{x}{x'} g(\frac{x}{x'}, Q^2) \qquad (3.1.10)$$

that is the conventional Altarelli-Parisi evolution of F_2 driven by $g \to q\bar{q}$

There are at least two reasons why the formulas (3.1.9) and (3.1.10) based on the leading $\log(Q^2)$ approximation are inadequate in the small x region. The first is due to Lipatov effect and the second arises from shadowing. We discuss these effects in turn. A crucial observation is that it is the dominance of the strong ordering of transverse momenta which leads to the nested integrations of (3.1.9). However at small x where the leading $\log(1/x)$ terms dominate it is important to retain the full Q^2 dependence and not just the leading $\log(Q^2)$ terms. This is accomplished by the Lipatov equation for the unintegrated gluon distribution f which sums the ladder diagrams over the full phase space of the transverse momenta and not simply the strongly ordered part. In the case of fixed $\bar{\alpha}_s$ the Lipatov equation can be solved analytically and the leading small x behaviour of $f(x,k_T^2)$ is given by the formula (2.2.10). We note, in particular, the factor $(k_T^2)^{1/2}$ which may be traced to the anomalous dimension having magnitude 1/2 [23]. Due to this factor the region of strongly ordered transverse momenta is no longer dominant. The integrals are no longer of logarithmic dk_T^2/k_T^2 form and we must use exact k_T^2 dependence of $F_2^{(0)}$ as well as integrating over the full region of phase space of transverse momenta.

At the very small x region the singular $x^{-\lambda}$ behaviour of f will be tamed by shadowing effects which lead to parton saturation (see Sec. 2.3). The saturation limit f_{sat} of f grows linarly with k_T^2 and so , as before, the k_T^2 behaviour requires that we must integrate over full phase space of transverse momenta [42].

Both the analytic solution of the Lipatov equation given by the formula (2.2.10) as well as the saturation limit overestimate their respective effects [25,26]. The numerical solution of the Lipatov equation shows, particularly when the effects of the running QCD coupling are included, that the approximate analytic form considerably overestimates the actual solution [26]. Secondly, the numerical solution of the Lipatov equation with the non-linear shadowing term included (see eq. (2.3.5)) shows that the saturation limit is approached rather slowly [26] and is irrelevant for $x > 10^{-4}$ which will be probed at HERA (see Sec.2.3). In order to obtain reliable prediction it is therefore necessary to use the "exact" (numerical) solution f of the Lipatov equation in the formula (3.1.7) and this calculation has been performed in the ref. [40].

In the analysis of the diagrams shown in Fig. .9 it is convenient to use the basic light-like momenta q' and p where $q' = q + xp$. We decompose the gluon and quark 4-momenta k and κ respectively, in terms of the Sudakov variables

$$k = ap - bq' + \mathrm{k}_T$$

$$\kappa = \alpha p - \beta q' + \boldsymbol{\kappa}_T \tag{3.1.11}$$

We must carry out the integration over the box diagrams subject to quark mass-shell constraints which, in terms of the Sudakov variables, are of the form:

$$(\alpha - x)(1-\beta)2pq - \kappa_T^2 = m_q^2$$
$$(a - \alpha)\beta 2pq - (\boldsymbol{\kappa}_T - \mathrm{k})^2 = m_q^2 \tag{3.1.12}$$

The contributions of the diagrams of Fig.9 to the functions $F_{T,L}(x, Q^2)$ are expressed in the form [40,41,43]:

$$F_T^0(x', k_T^2, Q^2) = 2\sum e_q^2 \frac{Q^2}{4\pi^2}\int_0^1 d\beta \int d^2\boldsymbol{\kappa}'_T \alpha_s(\kappa_T'^2 + m_{q0}^2)$$

$$*\{[\beta^2 + (1-\beta)^2][\frac{\kappa_T^2}{D_1^2} - \frac{\boldsymbol{\kappa}_T \cdot (\boldsymbol{\kappa}_T - \mathrm{k}_T)}{D_1 D_2}] + \frac{m_q^2}{D_1^2} - \frac{m_q^2}{D_1 D_2}]\}$$

$$*x'\delta\{x' - [1 + \frac{\kappa_T'^2}{Q^2}\beta(1-\beta) + \frac{k_T^2}{Q^2}]^{-1}\} \tag{3.1.13}$$

$$F_L^0(x', k_T^2, Q^2) = 2\sum e_q^2 \frac{Q^4}{\pi^2}\int_0^1 d\beta \int d^2\boldsymbol{\kappa}'_T \alpha_s(\kappa_T'^2 + m_{q0}^2)$$

$$*\beta^2(1-\beta)^2[\frac{1}{D_1^2} - \frac{1}{D_1 D_2}]x'\delta\{x' - [1 + \frac{\kappa_T'^2}{Q^2}\beta(1-\beta) + \frac{k_T^2}{Q^2}]^{-1}\} \tag{3.1.14}$$

where

$$D_1 = \kappa_T^2 + \beta(1-\beta)Q^2 + m_q^2 \tag{3.1.15}$$

$$D_2 = (\boldsymbol{\kappa}_T - \mathrm{k}_T)^2 + \beta(1-\beta)Q^2 + m_q^2 \tag{3.1.16}$$

$$\boldsymbol{\kappa}_T = \boldsymbol{\kappa}'_T + (1-\beta)\mathbf{k_T} \tag{3.1.17}$$

and $x' \geq x$. The parameter m_q denotes the quark mass while the "mass" m_{q0} serves as the regulator which "freezes" the coupling at $\alpha_s(m_{q0}^2)$ for small $\kappa_T'^2$. For the heavy quark contribution it may be set $m_{q0} = m_h$ where m_h is the mass of the heavy quark h.

For heavy quarks the formulas (3.1.7), (3.1.13) and (3.1.14) describe the photon-gluon fusion process which is expected to be the dominant one at small x. Those formulas are valid for arbitrary Q^2 including the region of small $Q^2 << m_h^2$. The cross-section for electroproduction of heavy quarks is in fact dominated by this "photoproduction" region.

In Fig. 10 we give results of the calculation for the structure functions $F_2(x,Q^2)$ and $F_L(x,Q^2)$ in the small x region relevant for HERA. We find, in particular, that the shadowing effects are very small.

3.2 Deep inelastic plus jet events as a probe of the QCD behaviour at small x.

There are several "dedicated" measurements of the small x physics which are aimed at revealing the QCD dynamics at small x. The deep inelastic lepton-hadron scattering containing a measured jet is one of the ideal processes for this purpose [26,27,44-48].

The idea is is to study deep inelastic (x,Q^2) events which contain an identified jet (x_j, k_{1T}^2) where $x << x_j$ and $Q^2 \simeq k_{1T}^2$. The process is illustrated in Fig. 11. Since we choose events with $Q^2 \simeq k_{1T}^2$ the QCD evolution (from k_{1T}^2 to Q^2) is neutralised and attention is focussed on the small x , or rather small x/x_j behaviour. The small x/x_j behaviour of the jet production is generated by the gluon radiation as shown in the diagram of Fig. 11a . Choosing the configuration $Q^2 \simeq k_{1T}^2$ we eliminate by definition the gluon emission which corresponds to strongly ordered transverse momenta i.e. that emission which is responsible for the QCD evolution (see Sec. 2.1). The measurement of jet production in this configuration may therefore test more directly the $(x/x_j)^{-\lambda}$ behaviour which is generated by Lipatov equation where the transerse momenta are not ordered (See Sec.2.2).

The differential transverse structure function for the process "$\gamma(Q^2)$" $+ p \rightarrow jet(x_j,k) + X$ may be written in the form:

$$x_j \frac{\partial^2 F_T(x,Q^2;x_j,k^2)}{\partial x_j \partial k^2} = \frac{3\alpha_s(k^2)}{\pi k^4}[\sum_a x_j f_a(x_j,k^2)]F(\frac{x}{x_j},k^2,Q^2) \qquad (3.2.1)$$

where , for convenience, we denote the transverse momentum of the jet as $k \equiv k_T$ and where, assuming the t-channel pole dominance the sum over the parton distributions is:

$$\sum_a f_a = g + \frac{4}{9}\Sigma \qquad (3.2.2)$$

with Σ given by (2.1.3). (Similar expression is obtained for the differential longitudinal structure function but, of course, with the different factor F). The factor F, which has the dimensions of k^2 represents the photon-gluon process shown by the upper blob in Fig. 11b; that is F/k^2 can be identified with the gluon structure function integrated over the longitudinal momentum of the gluon. At small $z = x/x_j$ the function F is given by the sum of ladder diagrams shown in Fig. 12. The function F satisfies the Lipatov equation of the following form:

$$-z\frac{\partial H(z,k^2,Q^2)}{\partial z} = K_L \otimes H \qquad (3.2.3)$$

with

$$H(z,k^2,Q^2) = \frac{3\alpha_s(k^2)}{\pi}F(z,k^2,Q^2) \qquad (3.2.4)$$

where the kernel K_L is defined by the eq.(2.2.2). The boundary condition for this equation at some $z = z_0$ ($z_0 < 1$) are given by the quark box (and crossed box) contribution $\bar{F}^{(0)}_{T,L}(k^2,Q^2)$ to the gluon+"γ" scattering (see Fig. 13). The functions $\bar{F}^{(0)}_{T,L}(k^2,Q^2)$ are defined in terms of $F^{(0)}_{T,L}(x',k^2,Q^2)$ given by the formulas (3.1.13) and (3.1.14)

$$\bar{F}^{(0)}_{T,L}(k^2,Q^2) = \int_0^1 \frac{dx'}{x'} F^{(0)}_{T,L}(x',k^2,Q^2) \qquad (3.2.5)$$

It is important to notice that the function $F(z,k^2,Q^2)$ is, in principle, exactly calculable within perturbative QCD (including its normalisation). When the running coupling constant effects are neglected then the leading small z behaviour of $F(z,k^2,Q^2)$ can be obtained analytically [26,43,45-47]

$$F(z,k^2,Q^2) = \frac{9\pi^2}{512}\frac{2\sum e_q^2 \bar{\alpha}_s^{1/2}}{\sqrt{21\zeta(3)/2}}(k^2Q^2)^{1/2}\frac{z^{-\lambda}}{\sqrt{ln(1/z)}}\{1+O[1/ln(1/z)]\} \qquad (3.2.6)$$

where λ is given by the eq.(2.2.9) and where $\bar{\alpha}_s = \alpha_s(Q^2)$. The analytic expression for the function F corresponding to the longitudinal structure function is is obtained from (3.2.6) after multiplying the right hand side by a factor 2/9. The analytic formula (3.2.6) however overestimates the magnitude of the function F (see Fig. 14) and so it is necessary to use the numerical solution of the Lipatov equation in order to get a reliable prediction.

Let us now discuss the feasibility of using the deep inelastic events which contain a meaured jet to identify the singular $z^{-\lambda}$ type of behaviour at HERA [27,45,46,48].

One practical limitation is that jets can only be measured if they are emitted at sufficiently large angles ($\theta_j > 5^0$) to the proton beam direction in the HERA laboratory frame. The relation between the kinematic variables describing the jet is illustrated by Fig. 15. We see that large x_j jets are only emitted at small θ_j; for a given θ_j we can reach larger x_j by observing jets with larger k_T^2 but with a depleted event rate. Fig. 16 shows the acceptance regions for these jets for various choices of the cuts on the jet variables x_j and θ_j (together with the constraints $\frac{1}{2}Q^2 < k_T^2 < 2Q^2$ and $z \equiv x/x_j < 0.1$).

In order to identify the Lipatov $z^{-\lambda}$ behaviour we need deep inelastic + jet events, with $k_T^2 \simeq Q^2$, over an interval of $z \equiv x/x_j$ which covers values of z as small as is experimentally possible. As a compromise we select the region $x_j > 0.05$ and $x < 2 * 10^{-3}$.

The differential cross section fo deep inelastic + jet production is given by:

$$\frac{\partial^2\sigma}{\partial x \partial Q^2} = \int dx_j \int dk_T^2 \frac{4\pi\alpha^2}{xQ^4}[(1-y)\frac{\partial^2 F_2}{\partial x \partial Q^2} + \frac{1}{2}y^2\frac{\partial^2(2xF_1)}{\partial x \partial Q^2}] \qquad (3.2.7)$$

where the differential structure functions are each given by equations of the form of (3.2.1) with the boundary conditions, $\bar{F}^{(0)}$, for F appropriate to $F_2 \equiv F_T + F_L$ and $2xF_1 \equiv F_T$. As usual $y = Q^2/xs$ where $\sqrt{s}$ is the CM energy of the incoming electron-proton system. Fig. 17 shows the predicted x dependence of the deep inelastic+jet cross-section relevant for HERA [48]. For reasons given above, the regions of integrations in (3.2.7) are restricted to $x_j > 0.05$ and $\theta_j > 5^0$, but subject to the additional constraint $\frac{1}{2}Q^2 < k_T^2 < 2Q^2$. The continuous curves give the values of the cross-section when the Lipatov effects are included. These are to to be contrasted with the dashed curves which show the values when the Lipatov effect is neglected, that is when just the quark box approximation is used to evaluate

$\partial^2 F_2/\partial x \partial Q^2$ and $\partial^2(2xF_1)/\partial x \partial Q^2$. The steep rise of the continuous curves with decreasing x (i.e. decreasing $z \equiv x/x_j$) reflects the $z^{-\lambda}$ Lipatov effect generated by the gluon radiation.

3.3 Deep inelastic diffraction.

The deep inelastic diffraction is the process $"\gamma"(Q^2) + p \to X + p$ with the large rapidity gap between the recoiled proton and the hadronic system X. It is assumed to be dominated by the pomeron exchange as illustrated in Fig. 18. The differential diffractive structure function is then related to the pomeron structure function F_2^P [49] ;

$$\frac{\partial^2 F_2^{diff}}{\partial t \partial \xi} = \frac{\beta^2(t)}{16\pi\xi} F_2^P(\frac{x}{\xi}, Q^2, t) \tag{3.3.1}$$

where $\xi = \delta q/pq$ and $t = \delta^2$. Note that the variable $x' = x/\xi$ is the Bjorken scaling variable corresponding to deep inelastic "scattering" on a pomeron since $x' = Q^2/2\delta q$. The function $\beta(t)$ is the pomeron coupling to the nucleon and we assume that the pomeron has its intercept equal to 1.

For large Q^2 the pomeron structure function F_2^P is related in a standard way to the quark (and antiquark) distributions in a pomeron

$$F_2^P(x', Q^2, t) = x \sum_i e_i^2 [q_i^P(x', Q^2, t) + \bar{q}_i^P(x', Q^2, t)] \tag{3.3.2}$$

It is usually assumed that pomeron consists predominantly of gluons [50-52]. The quark and antiquark distributions in a pomeron which define the pomeron structure function are generated radiatively by gluon conversion to $q\bar{q}$ pairs which in the first approximation is given by the Altarreli- Parisi equation:

$$Q^2 \frac{\partial q_i^P(x', Q^2, t)}{\partial Q^2} = \frac{\alpha_s(Q^2)}{2\pi} \int_{x'}^1 \frac{dy}{y} P_{gq}(\frac{x'}{y}) g^P(y, Q^2, t) \tag{3.3.3}$$

where $g^P(y, Q^2, t)$ is the gluon distribution in a pomeron which is assumed to saturate the momentum conservation sum-rule:

$$\int_0^1 dy y g^P(y, Q^2, t) = 1 \tag{3.3.4}$$

In other models [49] it is assumed on the basis of the pomeron-photon analogy that the pomeron couples directly to quarks. In this approach the quark distributions are not constrained to satisfy the momentum conservation sum rules.

If the pomeron has a large gluon component and if its radius R_P is assumed to be small (i.e. of the order of 0.1fm or so) then one may expect that the non-linear shadowing effects discussed in Sec. 2.3 can become very important [52]. This ccomes from the fact that the nonlinear shadowing terms are now proportional to $1/R_P^2$.

An interesting possibility was considered in refs.[53-57] that deep inelastic diffraction can be calculated almost entirely within perturbative QCD from triple gluonic ladder diagrams i.e. from the same diagrams which describe parton screening effects which we discussed in Sec. (2.3) (see.Fig. 19). The use of perturbative QCD can be justified in the analysis of large k_T jet production of the diffractively produced system (see Fig. 20). The measurement of jet production in the diffractively produced system can also be a complementary test of the gluon distributions at small x. The simplest process in this case is the diffractive production of two jets and the cross-section of this process is [55]

$$\frac{\partial^3\sigma^D}{\partial t\partial k_T^2\partial z} = [F_N^{2G}(t)]^2[x_j g(x_j,k_T^2)]^2 \sum_i e_i^2 \frac{4\pi^2\alpha_{em}}{3Q^2(k_T^2)^2}\alpha_s z^2(1-z)^2 \qquad (3.3.5)$$

where $z = x/(x+x_j)$ and $[F_N^{2G}(t)]$ is the two gluon-proton form-factor. The variable x_j denotes the longitudinal momentum fraction of the jet i.e. its four momentum k is

$$k \simeq x_j p + \mathbf{k}_T \qquad (3.3.6)$$

It may be seen that the cross section for jet production is very sensitive to gluon distribution being proportional to $[x_j g(x_j,k_T^2)]^2$.

4. SHADOWING IN LEPTON-NUCLEUS SCATTERING AT SMALL x.

The nuclear shadowing in inelastic lepton nucleus scattering describes the phenomenon in which the nuclear structure function (normalised per nucleon) is smaller than the structure function of a free nucleon [58-62]. The nuclear shadowing is a firmly established experimental fact both for heavy and for light nuclei [63-65]. It is a small x effect since it takes place for $x \leq 0.1$ or so (see Figs. 21 and 22). The data also suggest that shadowing persists to be present for large Q^2 (see Fig. 22b) i.e. in the region where the QCD improved parton model is expected to be applicable. The shadowing in deep inelastic scattering thus should reflect the shadowing effects in the quark (and antiquark) distributions in a nucleus. The shadowing effects are also of course expected to be present in the nuclear gluon distributions.

One can distinguish three regions of x where different phenomena responsible for nuclear shadowing can occur. On the basis of the uncertainty principle one finds that for $x < 1/(2MR_A)$ where M is the nucleon mass and R_A is the nuclear radius the partons can occupy longitudinal distances comparable to the nuclear radius and so the partons from different nucleons can spatially overlap and interact. This interaction of partons from different nucleons leads to reduction of the effective number of partons in a nucleus. It is in this region of x where the QCD shadowing effects discussed in Sec.(2.3) become important [66,67]. This region of the very small values of x ($x << 10^{-2}$ or so) is very interesting theoretically. It may be easily seen that if the equations discussed in the Sec. (2.3) are adapted to the nuclear case and written for the nuclear gluon distributions normalised per nucleon then the strength of the shadowing term is enhanced by a factor $A^{1/3}$. The QCD shadowing corresponding to recombination of partons from different nucleons in a nucleus becomes therefore stronger in the nuclear environment.

In the region of moderately small x where $1/(2MR_A < x < 1/(Mr)$ where r is the average distance between nucleons in a nucleus (i.e. $r \simeq 1fm$) one expects that the shadowing will decrease with increasing x. The x dependence of shadowing in this region is governed by the nuclear form-factor. Finally for $x > 1/(Mr)$ the shadowing is negligible.

The parton model is described by the "hand-bag" diagram for the virtual Compton scattering amplitude (Fig.23). It is this hand-bag structure of the diagram which guarantees Bjorken scaling (modulo perturbative QCD corrections) which guarantees Bjorken scaling independently of the structure of the lower part of this diagram. One can represent the diagram corresponding to the interaction of the virtual photon with the nucleus in a form of the multiple interaction series. Different terms in this series correspond to different number of nucleons participating in the interaction. The shadowing comes from those terms where at least two nucleons participate in the

interaction. Various models of shadowing correspond to the various structure details of the corresponding diagrams.

At small x one can assume that the multiple interaction diagrams are dominated by the pomeron exchange shown in Fig. 24. The contribution of the double interaction diagram can be then directly related to the pomeron structure function discussed in the Sec. (3.1) i.e.

$$\Delta F_{2A} = -8 \int_{\xi_0}^{1} \frac{d\xi}{\xi} \int d^2\mathbf{b} dz_1 dz_2 \Theta(z_1 - z_2) n_A(\mathbf{b}, z_1) n_A(\mathbf{b}, z_2) cos[M\xi(z_1 - z_2)]$$

$$\frac{\partial^2 F_2^{diff}}{\partial \xi \partial t} \simeq -\frac{\pi}{2} \int_{x}^{1} \frac{d\xi}{\xi} \int d^2\mathbf{b} dz_1 dz_2 \Theta(z_1 - z_2) n_A(\mathbf{b}, z_1) n_A(\mathbf{b}, z_2) cos[M\xi(z_1 - z_2)]$$

$$\beta^2(0) F_2^P(\frac{x}{\xi}, Q^2, t = 0) \tag{4.1}$$

where

$$\xi_0 = x(1 + M_{x0}^2) \tag{4.2}$$

and where M_{x0}^2 is the lowest mass squared of the diffractively produced system. The negative sign of the shadowing term is related to the fact that the amplitude of the diffractive scattering is imaginary. The definition of various variables and functions in the formula (4.1) is the same as in the Sec. (3.3) and the function $n_A(\mathbf{b}, z)$ is the nucleon number density of the nucleus at the point $(\mathbf{b}, z)$. It should be noted that the x' scaling of the pomeron structure function ($x' = x/\xi$) implies the Bjorken scaling of the shadowing term ΔF_{2A}

The double interaction diagram neglects the interaction of the diffractively produced system within the nucleus and this approximation leads to the overestimate of nuclear shadowing for heavy nuclei. There exist several approximate model dependent ways to take into account this interaction [62,68-70].

For low Q^2 the parton model and so the partonic mechanism of shadowing may not be applicable. In this low Q^2 region the natural mechanism of shadowing is that related to the vector meson dominance i.e. to the multiple scattering of vector-mesons which couple to virtual photons [58,59].

Let us finally consider, as the illustration, the shadowing in inelastic lepton deuteron scattering [71-73]. It is entirely given by the double interaction diagram (Fig.25b) and so it is free from the model dependent assumptions concerning the multiple rescattering of the diffractively produced system.

The deuteron structure function $F_{2D}(x,Q^2)$ is related in the following way to the proton and neutron structure functions $F_{2p}(x,Q^2)$ and $F_{2n}(x,Q^2)$ and to the shadowing term $\delta F_2(x,Q^2)$ normalised per nucleon:

$$F_{2D}(x,Q^2) = F_{2p}(x,Q^2) + F_{2n}(x,Q^2) - 2\delta F_2(x,Q^2) \tag{4.3}$$

with $\delta F_2(x,Q^2) \geq 0$

Quantitative estimate of the shadowing term in inelastic lepton-deuteron scattering is important and interesting at least for the following two reasons:

(a) The inelastic lepton-deuteron scattering serves as the unique tool for determining the neutron structure function F_{2n}. The recent measurements of the structure function ratios F_{2D}/F_{2p} performed by the New Muon Collaboration [74,75] are very precise and so even the relatively small shadowing term can in principle affect extraction of the neutron structure function from the experimental data. This can in turn affect determination of other quantities like for instance the Gottfried sum I_G:

$$I_G = \int_0^1 \frac{dx}{x}[F_{2p}(x,Q^2) - F_{2n}(x,Q^2)] \tag{4.4}$$

(b) In the region of very small values of $x < 10^{-2}$ and for large Q^2 which may become accessible in the possible HERA measurements the shadowing should reveal various QCD effects including, in particular, parton screening from two different nucleons in the deuteron.

As discussed above the double interaction term relates the shadowing to the deep inelastic diffractive production. This relation takes the following form for the deuteron:

$$\delta F_2(x,Q^2) = \int d^2\boldsymbol{\delta}_T \int_{\xi_0}^1 d\xi S_D(\boldsymbol{\delta}^2) \frac{\partial^2 F_2^{diff}}{\partial\xi\partial t} \tag{4.5}$$

In this formula $S(\boldsymbol{\delta}^2)$ is the deuteron form-factor and $\frac{\partial^2 F_2^{diff}}{\partial\xi\partial t}$ is the diffractive structure function (see Sec. 3.3). We define $\xi = 2\delta q/p_D q$ where δ is the four momentum corresponding to pomeron. We also have

$$t \simeq -\boldsymbol{\delta}^2 \tag{4.6}$$

and

$$\boldsymbol{\delta}^2 = \boldsymbol{\delta}_T^2 + M^2\xi^2 \tag{4.7}$$

The region of low M_x^2 where M_x is the mass of the diffractively produced system is dominated by the diiffractive production of low mass vector mesons. It is assumed to be described by the Vector Meson Dominance model. In this model

the contribution of the low-mass vector mesons to nuclear shadowing corresponds to double scattering of vector mesons which couple to virtual photons (Fig.26). The corresponding shadowing term $\delta F_{2D}^{(v)}$ is:

$$\delta F_{2D}^{(v)} = \frac{Q^2}{4\pi} \sum_v \frac{M_v^4 \delta\sigma_{vD}}{\gamma_v^2 (Q^2 + M_v^2)^2} \tag{4.8}$$

where M_v is the mass of the vector meson v and the constants γ_v^2 can be calculated from the leptonic width of the vector meson v [58,76]. The cross-section $\delta\sigma_{vD}$ is given by:

$$\delta\sigma_{vD} = \frac{1}{16\pi^2}\sigma_{vN}^2 \int d^2\boldsymbol{\delta}_T S_D(\boldsymbol{\delta}^2) \tag{4.9}$$

where now $\boldsymbol{\delta}^2 = \boldsymbol{\delta}_T^2 + M^2 x^2 (M_v^2/Q^2 + 1)^2$ and σ_{vN} is the total vector meson nucleon total cross-section. It can be seen from (4.8) that the double scattering of vector mesons gives vanishing contributions to shadowing in the large Q^2 limit.

In Fig.27 we plot the results for $\delta F_{2D} = \delta F_{2D}^v + \delta F_{2D}^p$ as functions of x for fixed Q^2. We also plot separately the vector meson δF_{2D}^v and parton mechanism δF_{2D}^p contributions. The partonic contribution to shadowing is defined by the eq.(4.5) and (3.3.1) and the parametrisation of the pomeron structure function is the same as in [71]. The pattern of x dependence changes weakly with Q^2. The x dependence is determined by the "$1/\xi$" diffractive spectrum (see eq. (3.3.1)) for small values of x and by the deuteron form-factor for higher values of x. The latter stems from the fact that the form-factor argument, $\boldsymbol{\delta}^2$, depends upon ξ. It can also be seen that the shadowing in deuteron is a weak (i.e. 2-3%) effect.

Using the results presented in Fig.27 we may estimate the contribution of shadowing to the Gottfried sum $\Delta I_G(x > x_{min}, Q^2)$ defined as:

$$\Delta I_G(x > x_{min}, Q^2) = -2 \int_{x_{min}}^{0.1} \frac{dx}{x} \delta F_{2D}(x, Q^2) \tag{4.10}$$

For $Q^2 = 4GeV^2$ and for $x_{min} = 0.004$ (i.e. for the values corresponding to experimental measurements [75]) we find

$$\Delta I_G(x > x_{min}, Q^2) = 4GeV^2) = -0.025 \tag{4.11}$$

The independent estimate of ΔI_G presented in [72] gives which is based on the different model of diffractive production gives $\Delta I_G = -0.043$.

It should be noticed that the relation between the Gottfried sum and the measured structure functions F_{2D} and F_{2p} in the presence of shadowing is as below:

$$I_G(x_{min}, x_{max}, Q^2) \equiv \int_{x_{min}}^{x_{max}} \frac{dx}{x}[F_{2p}(x,Q^2) - F_{2n}(x,Q^2)] =$$

$$\int_{x_{min}}^{x_{max}} \frac{dx}{x}[2F_{2p}(x,Q^2) - F_{2D}(x,Q^2)] + \Delta I_G(x > x_{min}, Q^2) \qquad (4.12)$$

The shadowing leads to negative ΔI_G i.e. to smaller I_G than that determined experimentally assuming no shadowing. The experimental measurements give for the first integral in the right hand side of the eq. (4.12) the value $I_G^{exp} = 0.227 \pm 0.007(stat.) \pm 0.014(syst.)$ for $x_{min} = 0.004$, $x_{max} = 0.8$ and $Q^2 = 4GeV^2$ [75].

Let us now discuss the possible QCD effects on shadowing for large Q^2 [71].

In the large Q^2 region the shadowing contribution $\Delta F_{2D} \equiv -2\delta F_{2D}$ is related to the shadowing terms Δq_i and $\Delta \bar{q}_i$ in the quark and antiquark distributions in the deuteron:

$$\Delta F_{2D}(x,Q^2) = x \sum_i e_i^2 [\Delta q_i(x,Q^2) + \Delta \bar{q}_i(x,Q^2) \qquad (4.13)$$

The shadowing terms Δg is also present in the gluon distribution in the deuteron.

There are two possible effects which can modify shadowing contributions to parton distributions:

(1) mild scaling violation induced by the QCD evolution,

(2) possible recombination of partons from different nucleons which gives additional terms in the evolution equations (see eqs. (3.4a)-(3.4c)). Those terms are sensitive upon small x behaviour of gluon distributions in the nucleon.

The evolution equations for the shadowing terms in parton distributions in the deuteron have the following form:

$$Q^2 \frac{\partial x \Delta g(x,Q^2)}{\partial Q^2} = \frac{\alpha_s(Q^2)}{2\pi} x[P_{gq} \otimes 2\sum_i \Delta q_i + P_{gg} \otimes \Delta g]$$

$$-\frac{9\alpha_s(Q^2)^2}{8Q^2} \int_x^1 \frac{d\xi}{\xi}[\xi g(\xi,Q^2)]^2 \int_0^\infty d\delta_T^2 2S_D(M^2\xi^2 + \delta_T^2) \qquad (4.14a)$$

$$Q^2\frac{\partial x\Delta q_i(x,Q^2)}{\partial Q^2}=\frac{\alpha_s(Q^2)}{2\pi}x[P_{qq}\otimes\Delta q_i+P_{qg}\otimes\Delta g]$$

$$-\frac{3\alpha_s(Q^2)^2}{80Q^2}[xg(x,Q^2)]^2\int_0^\infty d\delta_T^2 2S_D(M^2x^2+\delta_T^2)$$

$$+\frac{\alpha_s(Q^2)}{\pi Q^2}\int_x^1\frac{dx'}{x'}\frac{x}{x'}\gamma(\frac{x}{x'})x'G_H(x',Q^2) \qquad (4.14b)$$

$$Q^2\frac{\partial xG_H(x,Q^2)}{\partial Q^2}=-\frac{9\alpha_s(Q^2)^2}{8Q^2}\int_x^1\frac{d\xi}{\xi}[\xi g(\xi,Q^2)]^2\int_0^\infty d\delta_T^2 2S_D(M^2\xi^2+\delta_T^2) \quad (4.14c)$$

where $g(x,Q^2)$ is the gluon distribution in a nucleon. The terms quadratic in xg correspond to the recombination of gluons from two different nucleons in the deuteron (see Fig. 28).

The QCD corrections to shadowing become important in the region of very small values of x and for moderately large values of Q^2, that is in the kinematical range of the possible HERA measurements. They are displayed in Fig. 29 and compared with the prediction of the partonic mechanism without the QCD evolution effects. Two points are worthwhile to be noticed:

(1)Large amount of gluons in a Pomeron (see Sec. 3.3) implies relatively large shadowing term Δg in the gluon distributions in the deuteron. This term enhances the shadowing effects in the quark and antiquark distributions (and so in F_{2D}) through the $q\bar{q}$ radiation from the gluons which is generated by the QCD evolution.

(2)The parton recombination from two different nucleons is very sensitive to the gluon distributions in the nucleon at low x.

5. SUMMARY AND OUTLOOK.

In these lectures we have discussed the elements of the QCD expectations concerning the small x behaviour of parton distributions and possible phenomenological implications of those expectations for deep inelastic lepton - hadron scattering. When discussing the phenomenological implications we have, in particular , emphasised the role of the jet production in deep inelastic scattering which will be the "landmark" measurement of the small x physics. We have pointed out that HERA can in principle measure this process although this measurement would certainly be very difficult.

There have been several theoretical developments concerning the small x physics which we have not discussed in the sufficient detail but which are certainly very

topical and important. They are, in particular: the small x behaviour of the parton distributions in a photon [77], theoretical issues related to the factorisation theorem at small x [41,78], the problem of the unified treatment of the small and large x regions [22], properties of the final states in deep inelastic scattering at small x [79] , theoretical foundation of the GLR equation (see Sec. 2.3) which has recently been revisited in [80], possible role of the non-perturbative effects at small x [24,81-83], theoretical description of structure functions in the low Q^2, low x region [84-86].

Our discussion of nuclear shadowing in deep inelastic lepton scattering has also been rather brief and qualitative. There exist however excellent comprehensive articles which review this subject with the sufficient detail [58-62]. When discussisng the nuclear shadowing we have focussed our attention on the quantitative estimate of this effect in lepton-deuteron inelastic scattering exploring the connection between the shadowing effect and deep inelastic diffraction. We also quantified the role of the parton recombination which modifies the evolution equation for the shadowing terms in the parton distributions.

Our discussion has focussed almost entirely on the deep inelastic scattering at small x. The role of the small x physics does extend however far beyond the lepton-hadron interactions. Knowledge of parton distributions at small x is crucial for understanding the semihard interactions in high energy hadronic collisions. The next generation of hadronic colliders, such as SSC and LHC, will be capable of probing the parton distributions at still amaller values of x, where various effects discussed in our lectures will be significantly amplified.

Acknowledgments.

I wish to thank Willi Plessas for his kind invitation to lecture at the Schladming School and for very warm hospitality. I thank Adrian Askew, Barbara Badełek, Alan Martin and Peter Sutton for very enjoyable research collaboration on problems presented in those lectures. This research has been supported in part by the Polish Committee for Scientific Research Grant N0. 2 0198 91 01.

References.

[1] R.G. Roberts, "The Structure of the Proton. Deep Inelastic Scattering", Cambridge University Press, Cambridge, New York, Port Chester, Melbourne, Sydney, 1990.

[2] W.J. Stirling, These Proceedings.

[3] G. Altarelli, Phys. Rep. **81** (1982) 1.

[4] E. Reya, Phys. Rep. **69** (1981) 195.

[5] Yu.L. Dokshitzer, D.I. Dyakonov and S.I. Troyan, Phys. Rep. **58** (1980) 265.

[6] L.V. Gribov, E.M. Levin and M.G. Ryskin, Phys. Rep. **100** (1983) 1.

[7] E.M. Levin, "Parton Density at Small x_B", Review talk at "QCD - 20 Years Later", Aachen, June 9-13, 1992, DESY preprint DESY 92-122.

[8] A.D. Martin, Acta. Phys. Polon. **B22** (1991) 1093; talk at 22nd International Symposium on Multiparticle Dynamics, Santiago de Compostela, Spain, July 1992.

[9] B. Badełek, K. Charchuła, M. Krawczyk and J. Kwieciński, Rev. Mod. Phys. **64** (1992) 927.

[10] Proceedings of the Topical Workshop on the Small x Behaviour of Deep Inelastic Scattering Structure Functions in QCD, DESY, Hamburg, Germany, May 1990, Nucl. Phys. B (Proc. Suppl.) **18C** (1990) 172.

[11] Proceedings of the Workshop "Physics at HERA", DESY, Hamburg, Germany, October 1992, edited by W. Buchmüler and G. Ingelman.

[12] G. Wolf, These Proceedings.

[13] J. Feltesse, "HERA, The New Frontier" (Presented at SLAC Summer Institute, Stanford, CA, USA, August 1991) Saclay preprint DAPNIA-SPP-92-01.

[14] G. Altarelli and G. Parisi, Nucl. Phys. **B126** (1977) 298.

[15] E.A. Kuraev, L.N. Lipatov and V.. Fadin, Zh. Ekssp. Teor. Fiz. **72** (1977) 373 [Sov. Phys. JETP **45** (1977) 199].

[16] Ya. Ya. Balitskij and L.N. Lipatov, Yad. Fiz. **28** (1978) 1597 [Sov. J. Nucl. Phys. **28** (1978) 822].

[17] L.N. Lipatov, in "Perturbative QCD", edited by A.H. Mueller, (World Scientific, Singapore, 1989), p.411.

[18] J.B. Bronzan and R.L. Sugar, Phys. Rev. **D17** (1978) 585.

[19] T. Jaroszewicz, Acta. Phys. Polon. **B11** (1980) 965.

[20] M. Ciafaloni, Nucl. Phys. **296** (1988) 49.

[21] S. Catani, F. Fiorani and G. Marchesini, Phys. Lett. **B234** (1990) 339; Nucl. Phys. **B336** (1990) 18.

[22] G. Marchesini, Proceedings of the Workshop "QCD at $200TeV$", Erice, Italy, June 1990, edited by L. Cifarelli and Yu.L. Dokshitzer, Plenum Press, New York, 1992, p. 183.

[23] T. Jaroszewicz, Phys. Lett. **B116** (1982) 291.

[24] R.E. Hancock and D.A. Ross, Nucl. Phys. **B383** (1992) 575.

[25] J. Kwieciński, A.D. Martin and P.J. Sutton, Phys. Rev. **D44** (1991) 260.

[26] J. Kwieciński, A.D. Martin and P.J. Sutton, Phys. Rev. **D46** (1992) 921.

[27] A.D. Martin, J. Kwieciński and P.J. Sutton, Nucl. Phys.B (Proc. Suppl.) **29A** (1992) 67.

[28] D. Strózik-Kotlorz, Z.Phys. **C53** (1992) 93.

[29] A.H. Mueller, Nucl. Phys. **B335** (1990) 115.

[30] E.M. Levin and M.G. Ryskin, Phys. Rep. **189** (1990) 267.

[31] A.H. Mueller, Nucl. Phys.B (Proc. Suppl.) **18C**(1990) 125.

[32] J. Kwieciński, A.D. Martin and P.J. Sutton, Phys. Lett. **B264** (1991) 199.

[33] A.H. Mueller and J. Qiu, Nucl. Phys. **B268** (1986) 427.

[34] J. Bartels and E.M. Levin, Nucl. Phys. **B387** (1992) 617.

[35] J. Bartels, J. Blümlein and G. Schuler, Z.Phys. **C50** (1991) 91.

[36] J.C. Collins and J. Kwieciński, Nucl. Phys. **B335** (1990) 89.

[37] E.M. Levin, G. Marchesini, M.G. Ryskin and B.R. Webber, Nucl. Phys. **B357** (1991) 167.

[38] J. Kwieciński, A.D. Martin, R.G. Roberts and W.J. Stirling, Phys. Rev. **D42** (1990) 3645.

[39] A.D. Martin, R.G. Roberts and .J. Stirling, "New Information on Parton Distributions", Durham Univ. preprint DTP/92/16 (RAL-92-021).

[40] A.J. Askew, J. Kwieciński, A.D. Martin and P.J. Sutton, "QCD Predictions for Deep Inelastic Structure Functions at HERA", Durham Univ. preprint DTP/92/78.

[41] S. Catani, M. Ciafaloni and F. Hautman, Phys. Lett. **B242** (1990) 91; Nucl. Phys. **B366** (1991) 135.

[42] E.M. Levin and M.G. Ryskin, Yad. Fiz. **53** (1991) 1052.

[43] S. Catani, M. Ciafaloni and F. Hautman, Proceedings of the Workshop "Physics at HERA", DESY, Hamburg, Germany, October 1992, edited by W. Buchmüler and G. Ingelman.

[44] A.H. Mueller, J.Phys. **G17** (1991) 1443.

[45] J. Bartels, M. Besancon, A. De Roeck and J. Kurzhoefer, "Measurements of Hot Spots at HERA", Proceedings of the Workshop "Physics at HERA", DESY, Hamburg, Germany, October 1992, edited by W. Buchmüler and G. Ingelman.

[46] J. Bartels, M. Loewe and A. De Roeck, Z. Phys. **C54** (1992) 635; A. de Roeck Nucl. Phys. B (Proc. Suppl.) **29A** (1992) 61;

[47] W.K. Tang, Phys. Lett. **B278** (1992) 363.

[48] J. Kwieciński, A.D. Martin and P.J. Sutton, Phys. Lett. **B287** (1992) 254.

[49] A. Donnachie and P.V. Landshoff, Nucl. Phys. **B244** (1984) 322; Phys. Lett. **B191** (1987) 309. ; Nucl. Phys. **B303** (1988) 634.

[50] G. Ingelman and P. Schlein, Phys. Lett. **B152** (1985) 256.

[51] E.L. Berger, J.C. Collins, D.E. Soper and G. Sterman, Nucl. Phys. **B286** (1987) 704.

[52] G. Ingelman and K. Janson-Prytz, Proceedings of the Workshop "Physics at HERA", DESY, Hamburg, Germany, October 1992, edited by W. Buchmüler and G. Ingelman; Nucl. Phys. B (Proc. Suppl.) **29A** (1992) 97.

[53] J. Bartels and G. Ingelman Phys. Lett. **B235** (1990) 175; G. Ingelman, Nucl. Phys. B(Proc. Suppl.) **18C** (1990) 172.

[54] M.G. Ryskin, Sov. J. Nucl. Phys., **52** (1990) 529.

[55] M.G. Ryskin, Proceedings of the Workshop "Physics at HERA", DESY, Hamburg, Germany, October 1992, edited by W. Buchmüler and G. Ingelman.

[56] N.N. Nikolaev and B.G. Zakharov, Z. Phys. **C53** (1992) 331.

[57] E.M. Levin and W. Wüsthoff, "Photon Diffractive Dissociation In Deep Inelastic Scattering", DESY preprint DESY 92-166.

[58] T.H. Bauer et al.,Rev. Mod. Phys. **50** (1978) 261.

[59] G. Grammer Jr. and J.D. Sullivan, in Electromagnetic Interactions of Hadrons, ed. A. Donnachie and G. Shaw, (Plenum, New York, 1978).

[60] L. Frankfurt and M. Strikman, Phys. Rep. **160** (1988) 235.

[61] R.J.M. Covolan and E. Predazzi, lectures at the Folgaria Winter School, February 1990, Univ. of Torino preprint DFTT 21/90.

[62] M. Arneodo, "Nuclear Effects in Structure Functions", CERN preprint CERN-PPE/92-113.

[63] EMC, M. Arneodo et al., Nucl. Phys. **B333** (1990) 1.

[64] NMC, P. Amaudruz et al., Z.Phys. **C51** (1991) 387.

[65] E-665, M.R. Adams et al., Fermilab-Pub-92-51-E.

[66] E.M. Levin and M.G. Ryskin, Yad. Fiz. **41** (1985) 472.

[67] J. Qiu, Nucl. Phys. **B291** (1987) 746.

[68] L.L. Frankfurt and M.I. Strikman, Nucl. Phys. **316** (1989) 340.

[69] S.J. Brodsky and H.J. Lu, Phys. Rev. Lett. **64** (1990) 1342.

[70] J. Kwieciński, Z.Phys. **C45** (1990) 461.

[71] B. Badełek and J. Kwieciński, Nucl. Phys. **B370** (1992) 278; Nucl. Phys. B (Proc. Suppl.) **29 A** (1992) 30.

[72] V.R. Zoller, Phys. Lett. **B279** (1992) 145; Z.Phys. **C54** (1992) 425.

[73] W. Melnitchouk and A.W. Thomas, "Shadowing in Deuterium", Univ. of Adelaide preprint ADP-92-192/T120.

[74] NMC, D. Allasia et al., Phys. Lett. **B249** (1990) 366.

[75] NMC, P. Amaudruz et al., Phys. Rev. Lett. **66** (1991) 387.

[76] J. Kwieciński and B. Badełek, Z.Phys., **C43** (1989) 251.

[77] J.R. Forshaw and P.N. Harriman, Phys. Rev. **D46** (1992) 3778.

[78] J.C. Collins and R.K. Ellis, Nucl. Phys. **360** (1991) 3.

[79] B.R. Webber, Proceedings of the Workshop "Physics at HERA", DESY, Hamburg, Germany, October 1992, edited by W. Buchmüler and G. Ingelman.

[80] J. Bartels, "Unitarity Corrections to the Lipatov Pomeron and the Small x Region in Deep Inelastic Scattering", DESY preprint DESY-92-114.

[81] P.V. Landshoff and O. Nachtman, Z. Phys. **C35** (1987) 405.

[82] J.R. Cudell, A. Donnachie and P.V. Landshoff, Nucl. Phys. **B322** (1989) 55.

[83] A. Donnachie and P.. Landshoff, Nucl. Phys. **B311** (1989) 509.

[84] B. Badełek and J. Kwieciński, Phys. Lett. **B295** (1992) 263.

[85] H. Abramowicz et al., Phys. Lett. **B269** (1991) 465.

[86] M. Glück, E, Reya and A. Vogt, Z. Phys. **C48** (1990) 471; **C53** (1992) 127.

Figure Captions.

Fig.1 The ladder diagram for the deep inelastic scattering in the LLQ^2 approximation.

Fig.2 The ladder diagram for the unintegrated gluon distribution $f(x,k^2)$ in the LL$1/x$ approximation.

Fig.3 (a) Diagrammatic representation of the quadratic shadowing term in the evolution equation (2.3.5). The box represents all possible perturbative QCD diagrams which couple 4 gluons to 2 gluons. The lower elongated blob represents

the coupling of the hadron to the gluon ladders; the two possibilities for this couplings are shown in Fig. 4. (b) An example of a QCD coupling 4 gluons to 2 gluons.

Fig.4 Two possibilities for the coupling of the hadron (i.e.proton) to the gluon ladders. In Fig. (a) the ladders arise from distinct constituents of the hadron, and in (b) from the same constituent.

Fig.5 Diagrams giving rise to shadowing terms in the evolution equations, (3.1.5 a-c), for the sea quark distributions.

Fig.6 (a),(b): The values of $xg(x,Q^2)$ at (a) $Q^2 = 4GeV^2$ and (b) $Q^2 = 20GeV^2$ calculated from the solution $f(x,k^2)$ of the integro-differential Lipatov equation (2.3.5). The three curves are, in descending order, the solution with shadowing neglected and the solutions with the shadowing term included with $R = 5GeV^{-1}$ and $R = 2GeV^{-1}$. (c) and (d) show the values of W' defined as the ratio of the quadratic to the linear term in the rhs. of the eq. (2.3.5). The values of shadowing correspond to the solutions with shadowing shown in (a) and (b) (from [25]).

Fig.7 A sketch of the characteristic curves, $y(\xi)$, obtained by solving the characteristic equations ccorresponding to the eq. (2.3.8), using input at $\xi = \xi_0$. In this approximation the gluon packing fraction parameter $W' \simeq \alpha_s(Q^2)$ on the critical line. In regions where shadowing is negligible the characteristic curves are straight lines (from [25]).

Fig.8 The structure function F_2 as a function of x at $Q^2 = 20GeV^2$ based on MRS partons [39]. Sets D_- and D_0 have the input gluon and sea quark distributions (multiplied by x) which behave respectively as $x^{-1/2}$ and x^0 at small x. The dashed curves show the effect of parton shadowing for two different choices of the parameter R.

Fig.9 (a) Diagrammatic representation of a gluon ladder contribution to the deep inelastic structure functions of the proton. q, κ, k and p denote the particle 4-momenta. (b) Diagrammatic representation of the factorisation formula of eq. (3.1.7). (c) Diagrams giving the small x behaviour of the structure functions for deep-inelastic electron-proton scattering.

Fig.10 Perturbative QCD predictions of the behaviour of the structure functions $F_2(x,Q^2)$ and $F_L(x,Q^2)$ at $Q^2 = 20GeV^2$ and small x [40]. The continuous curves are with shadowing neglected, while the upper (lower) dashed curves have shadowing effects included with $R = 5GeV^{-1}$ ($R = 2GeV^{-1}$). For the upper three curves the infrared cut-off in (2.2.2) and in (3.1.7) is chosen to be $k_0^2 = 1GeV^2$ while the lower of the two continuous curves give the unshadowed result for $k_0^2 = 2GeV^2$. The dot-dashed curves are the background contributions.

Fig.11 (a) Diagrammatic representation of a deep-inelastic event which contains an identified jet with longitudinal and transverse momentum $x_j p$ and k_{1T}, respectively. x_j is chosen as large as experimentally feasible ($x_j \sim 0.1$) and so we assume strong ordering of the longitudinal, as well as transverse, momentum at the parton a - gluon vertex. Parton a can be either a quark or a gluon. (b) The diagram giving the cross section for deep inelastic scattering events containing an identified jet of longitudinal and transverse momentum $x_j p$ and k, respectively.

Fig.12 The leading $\log(x_j/x)$ approximation to the process shown in Fig. 11.

Fig.13 The two diagrams embodied in the quark box diagram of Fig. 12.

Fig.14 The photon-gluon structure function factor $F(z, k^2, Q^2)$ corresponding to the transverse differential structure function for deep inelastic(x, Q^2) events with an identified jet (x_j, k^2), as a function of $z = x/x_j$ [26]. The continuous curves are calculated from the integro-differential form (3.2.3) of the Lipatov equation. for three different choices of the transverse momentum cutoff, $k_0^2 = 1, 2$ and $4GeV^2$, respectively. The solution is matched to the quark box driving term at $z = z_0 = 0.1$. The dashed curve shows the analytic leading $\log(z_0/z)$ approximation, eq. (3.2.6).

Fig.15 The relation between the jet kinematic variables for deep inelastic + jet events with $x = 5 * 10^{-3}$ and $Q^2 = 20GeV^2$ [45,46,48]. θ_j, the jet angle to the proton direction in the HERA laboratory frame, is not uniquely specified by $(x, Q^2; x_j, k_T^2)$. Varying the remaining azimuthal angle transforms the lines of constant θ_j into narrow bands in the x_j, k_T^2 plane. The lines shown are obtained by averaging over the azimuthal degree of freedom. The cross-sections shown in Fig. 17 correspond to jets lying in the shaded band , but subject to the additional constraint $\frac{1}{2}Q^2 < k_T^2 < 2Q^2$.

Fig.16 The acceptance region for deep-inelastic + jet events at HERA [48]. The dashed curves outline the acceptance regions for the dedected electron ($8^0 < \theta_e < 172^0$), whilst the solid curves outline the triangular acceptance region for jets with different kinematic x_j, θ_j cuts applied (together with the constraint $\frac{1}{2}Q^2 < k_T^2 < 2Q^2$ and $z \equiv x/x_j < 0.1$).

Fig.17 The cross section, $< \sigma >$ in pb, for deep inelastic + jet events shown as the function of x for three different bins of Q^2 [48]. The continuous curves show $< \sigma >$ calculated with the inclusion of the Lipatov soft gluon summation, i.e. with the full $F(z, k^2, Q^2)$. The corresponding $< \sigma >$ values calculated with just the quark box approximation $F = \bar{F}^{(0)}$ are shown as the dashed curves and, for clarity, each is joined with its associated solid curve by a vertical line.

Fig.18 Pomeron structure function in deep inelastic diffraction.

Fig.19 The triple gluon ladder contribution to deep inelastic diffraction.

Fig.20 The diagram representing the diffractive production of jets.

Fig.21 Compilation of structure function ratios for different nuclei (from [62]).

Fig.22 The Xe to D cross-section ratio shown (a) as the function of x and (b) as the function of Q^2 (from [62]).

Fig.23 The "hand-bag" diagram for the deep inelastic lepton-nucleus scattering. The lines in the upper part of this diagram denote quarks (or antiquarks).

Fig.24 The double Pomeron exchange contribution to shadowing in deep inelastic lepton - nucleus scattering. The dots represent other contributions to shadowing in which more than two nucleons participate in the ineraction . Those terms correspond to multiple rescattering of the diffractively produced system within the nucleus.

Fig.25 Handbag diagrams for single (a) and double (b) interaction for the virtual Compton scattering on a deuteron. The lines in the lower part of the diagrams denote nucleons while those in the upper part denote quarks (antiquarks).

Fig.26 Double scattering of vector mesons.

Fig.27 Results for δF_{2D} as functions of x for fixed values of Q^2 (continuous lines) [71]. The dotted curves mark the $\delta F_{2D}^{(p)}$ contributions and the dashed lines the $\delta F_{2D}^{(v)}$ contributions.

Fig.28 The two gluon ladder exchange for the double interaction diagram. The upper blob denotes different perturbative QCD couplings of the four gluons to the $q\bar{q}$ pair.

Fig.29 Effects of the QCD evolution on δF_{2D} for $Q^2 = 10GeV^2$ [71]. Long dashed curve shows unevolved δF_{2D} while remaining four lines show effects of the QCD evolution starting from $Q^2 = 4GeV^2$. Continuous line corresponds to the evolution without the parton recombination terms in the eqs. (4.14). The other three lines show the effects of the QCD evolution with the recombination terms included and correspond to three different gluon distributions in a nucleon: the short dashed line corresponds to $xg(x,Q^2) \to const$ for $x \to 0$, the dotted line corresponds to the gluon distribution containing both the singular $x^{-1/2}$ behaviour and shadowing effects while the dashed dotted line shows results for $xg(x,Q^2) \to x^{-1/2}$.

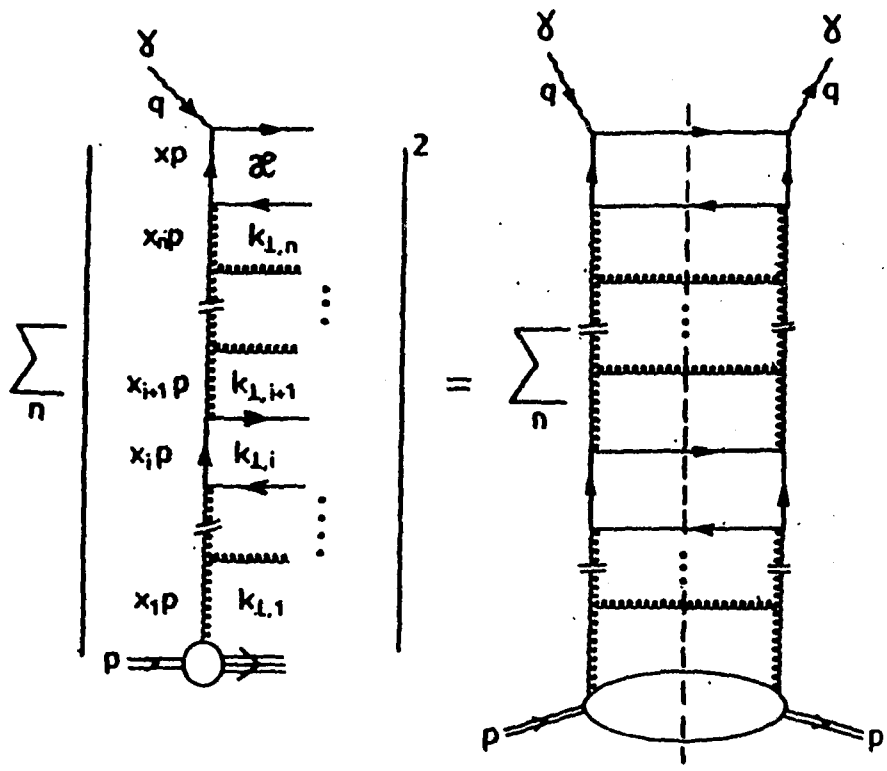
γ
q
xp
æ
x_n p
k_⊥,n
x_{i+1} p
k_⊥,i+1
x_i p
k_⊥,i
x_1 p
k_⊥,1
p
2
=
n
γ
γ
q
q
p
p

Fig.1

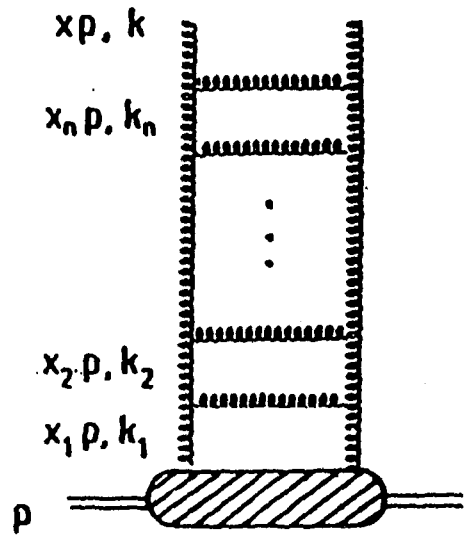
xp, k
x_n p, k_n
x_2 p, k_2
x_1 p, k_1
p

Fig.2

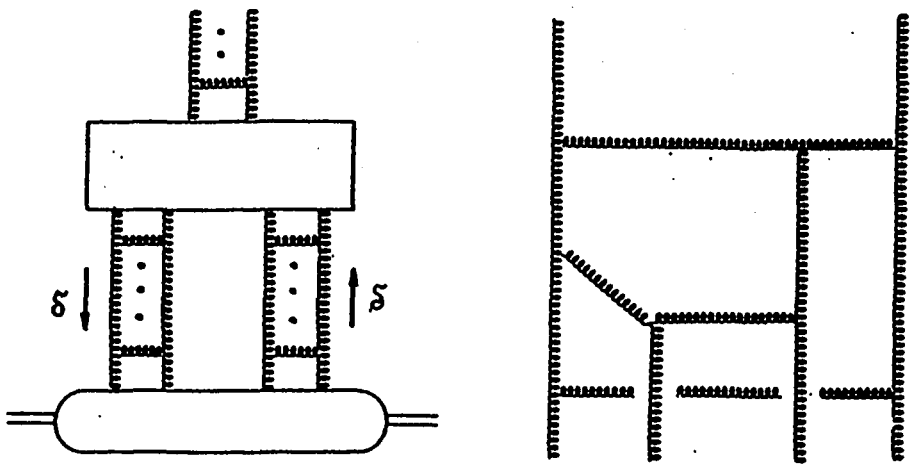

Fig.3

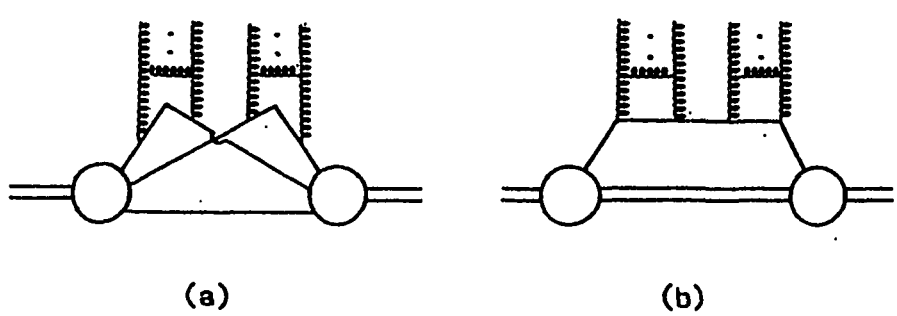

Fig.4

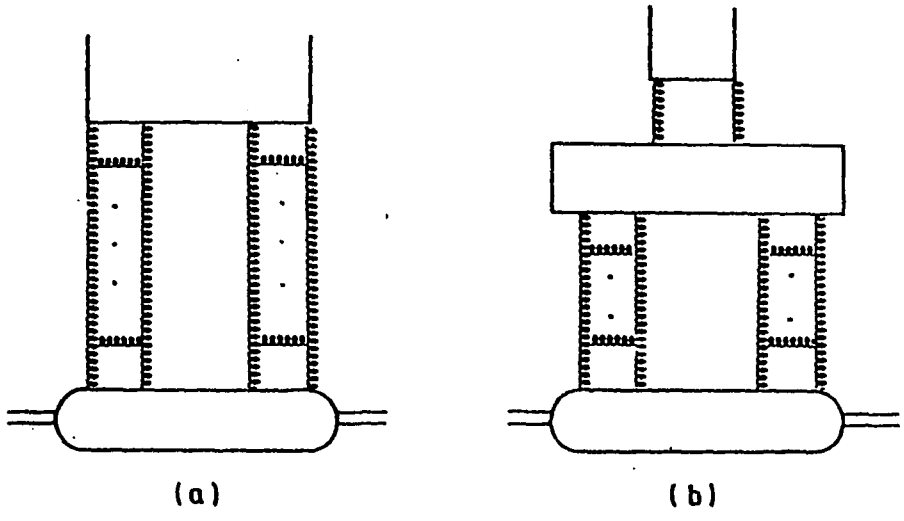
(a)
(b)

Fig.5

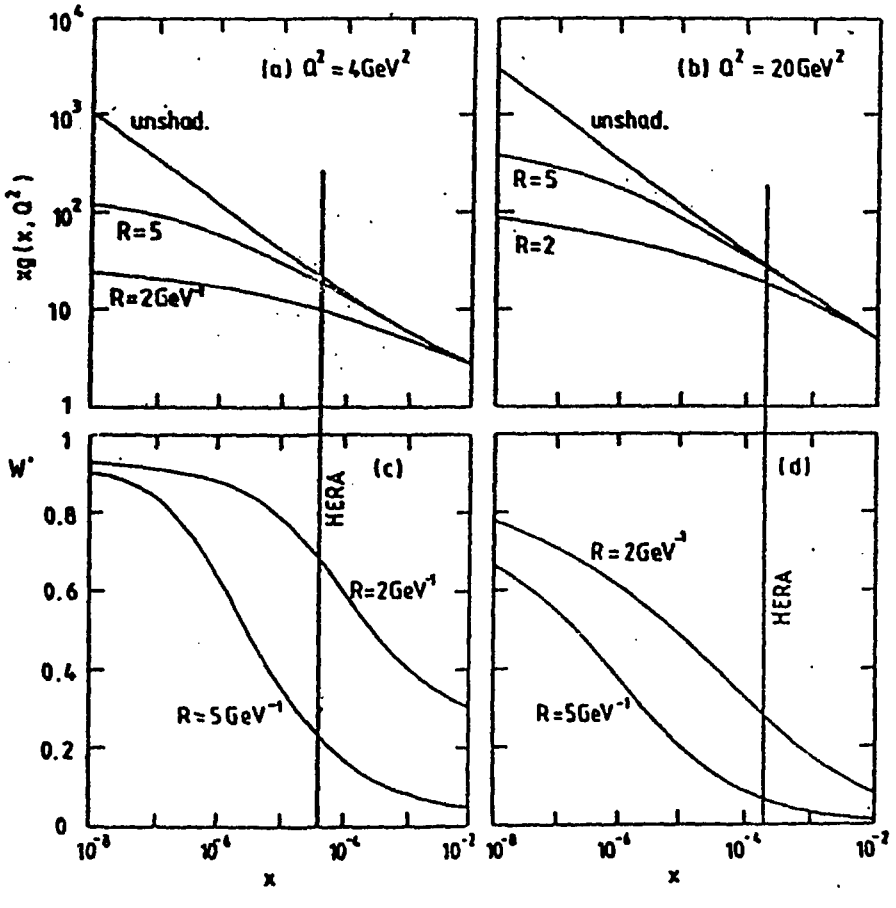
(a) $Q^2 = 4GeV^2$
(b) $Q^2 = 20GeV^2$
unshad.
R=5
R=2GeV^{-1}
R=2
$xg(x,Q^2)$
(c)
(d)
HERA
R=2GeV^{-1}
R=5GeV^{-1}
W'
x

Fig.6

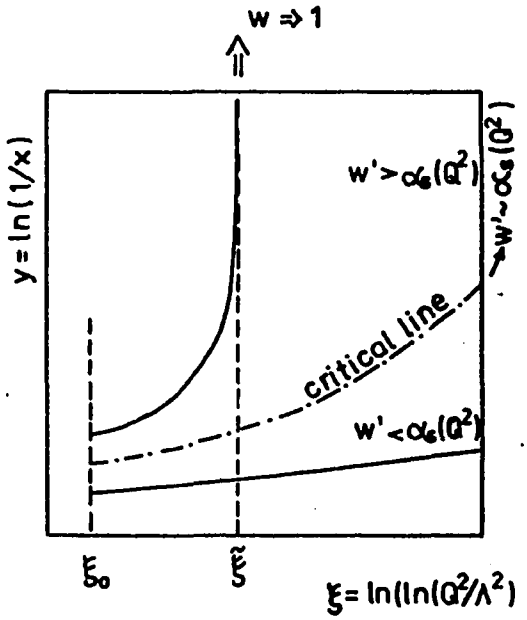
w ⇒ 1
y = ln(1/x)
w' > α_s(Q²)
w' ~ α_s(Q²)
critical line
w' < α_s(Q²)
ξ_0
ξ̃
ξ = ln(ln(Q²/Λ²))

Fig.7

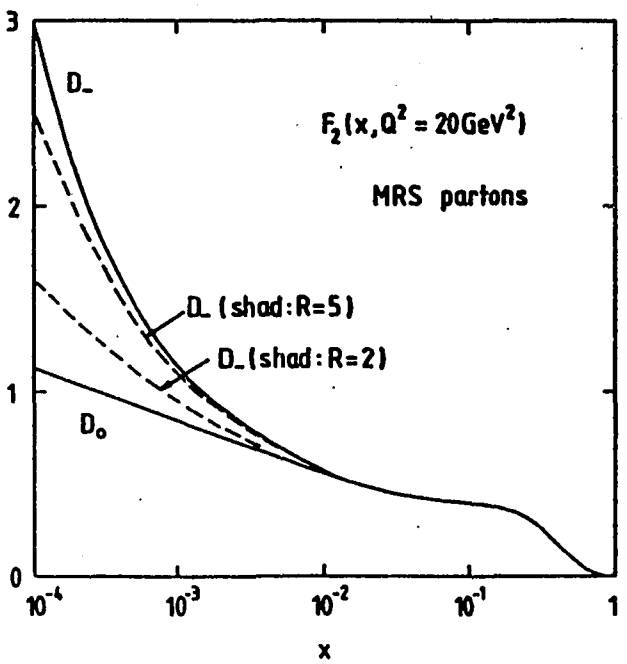
3
2
1
0
D_
F_2(x, Q² = 20GeV²)
MRS partons
D_ (shad: R=5)
D_ (shad: R=2)
D_0
10^-4
10^-3
10^-2
10^-1
1
x

Fig.8

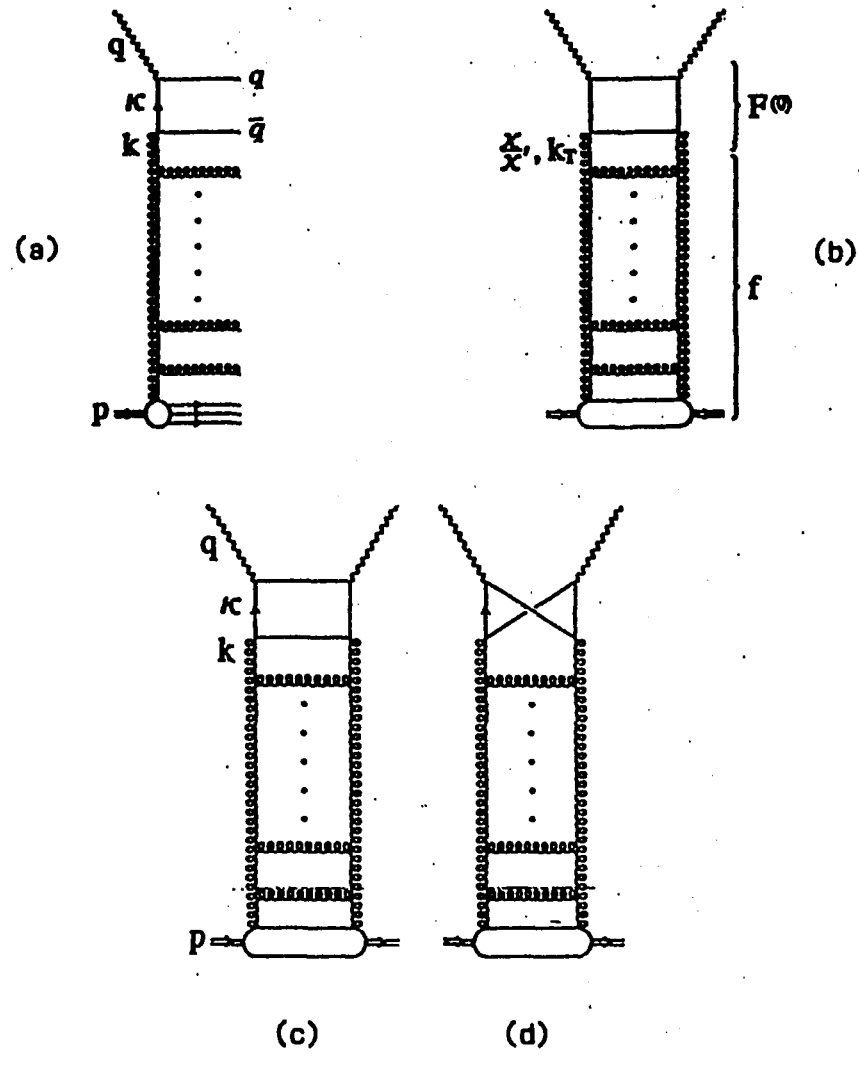

Fig. 9

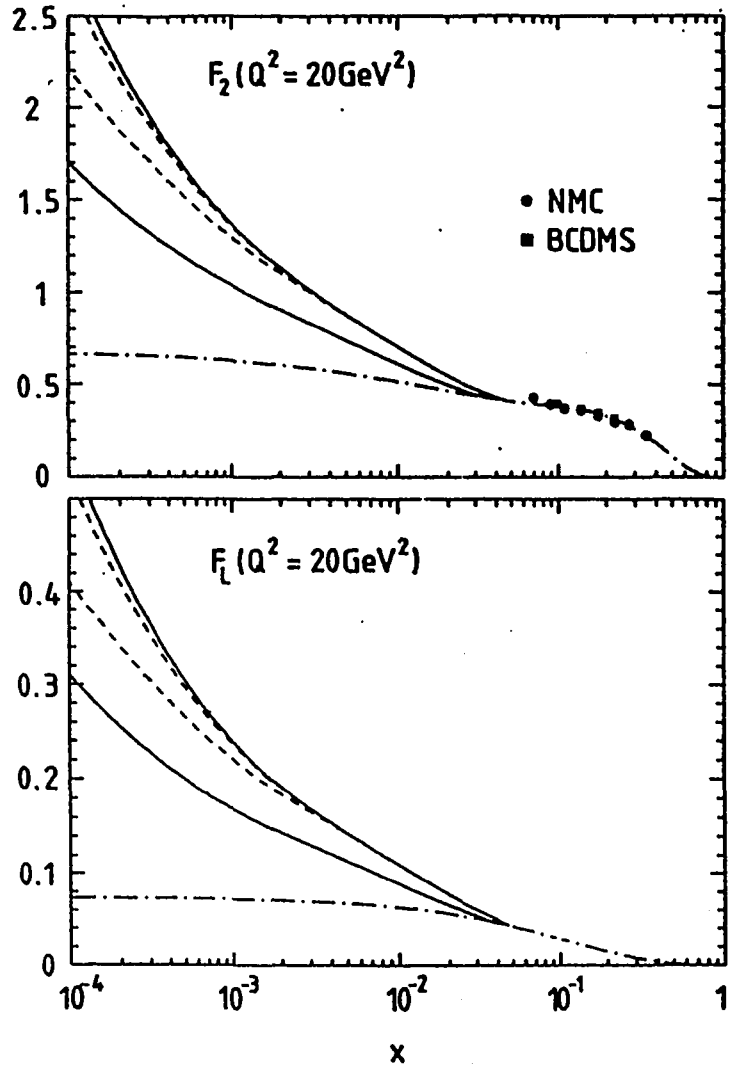
$F_2(Q^2 = 20GeV^2)$
• NMC
■ BCDMS
$F_L(Q^2 = 20GeV^2)$
2.5
2
1.5
1
0.5
0
0.4
0.3
0.2
0.1
0
10^{-4}
10^{-3}
10^{-2}
10^{-1}
1
x

Fig.10

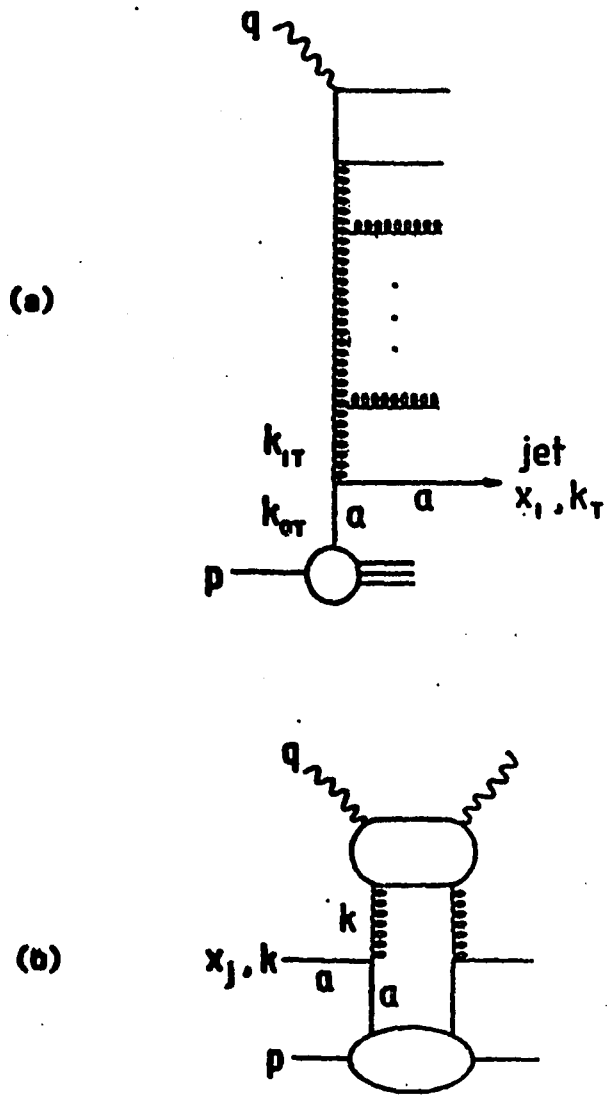

Fig.11

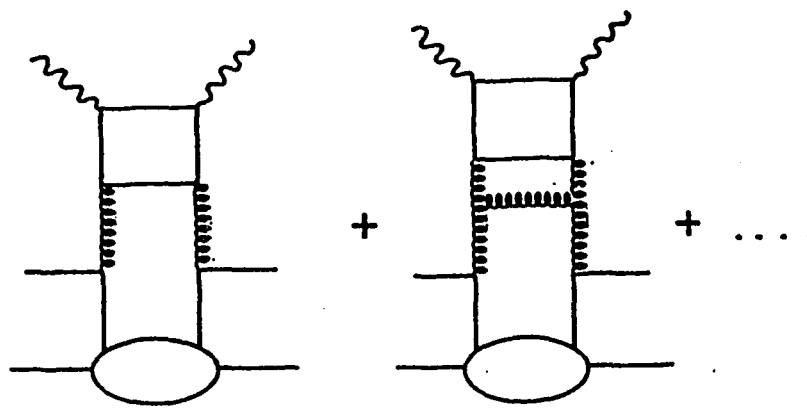

Fig.12

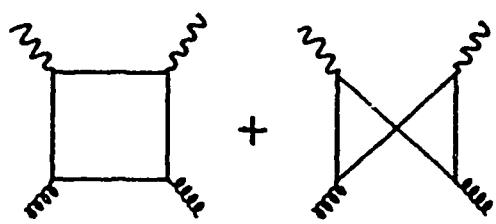

Fig.13

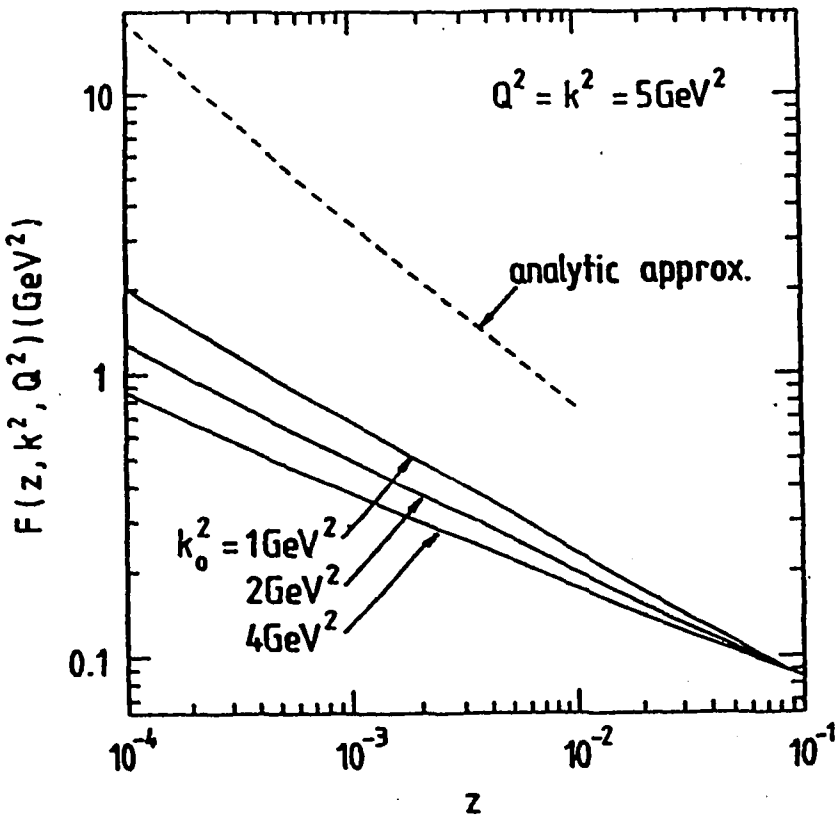
$Q^2 = k^2 = 5GeV^2$
analytic approx.
$k_o^2 = 1GeV^2$
$2GeV^2$
$4GeV^2$
$F(z, k^2, Q^2)$ (GeV^2)
10
1
0.1
10^{-4}
10^{-3}
10^{-2}
10^{-1}
z

Fig.14

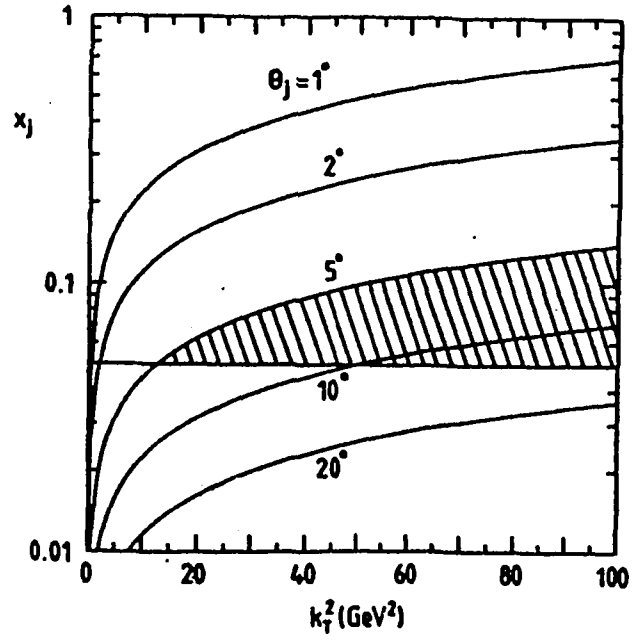
$\theta_j = 1°$
2°
5°
10°
20°
x_j
1
0.1
0.01
0
20
40
60
80
100
k_T^2 (GeV^2)

Fig.15

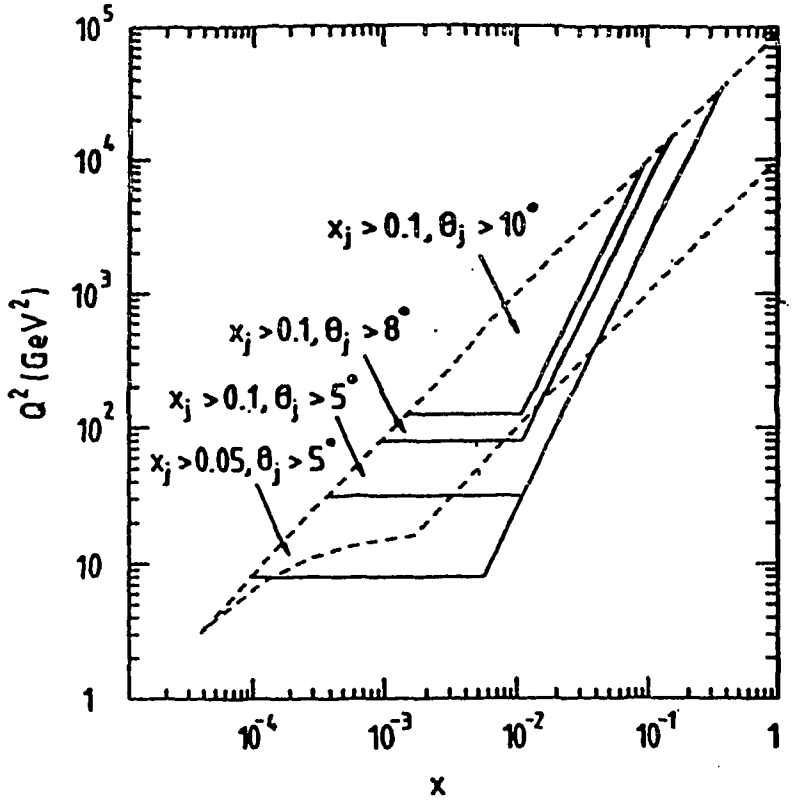
10^5
10^4
10^3
10^2
10
1
Q^2 (GeV^2)
$x_j > 0.1, \theta_j > 10°$
$x_j > 0.1, \theta_j > 8°$
$x_j > 0.1, \theta_j > 5°$
$x_j > 0.05, \theta_j > 5°$
10^{-4}
10^{-3}
10^{-2}
10^{-1}
1
x

Fig.16

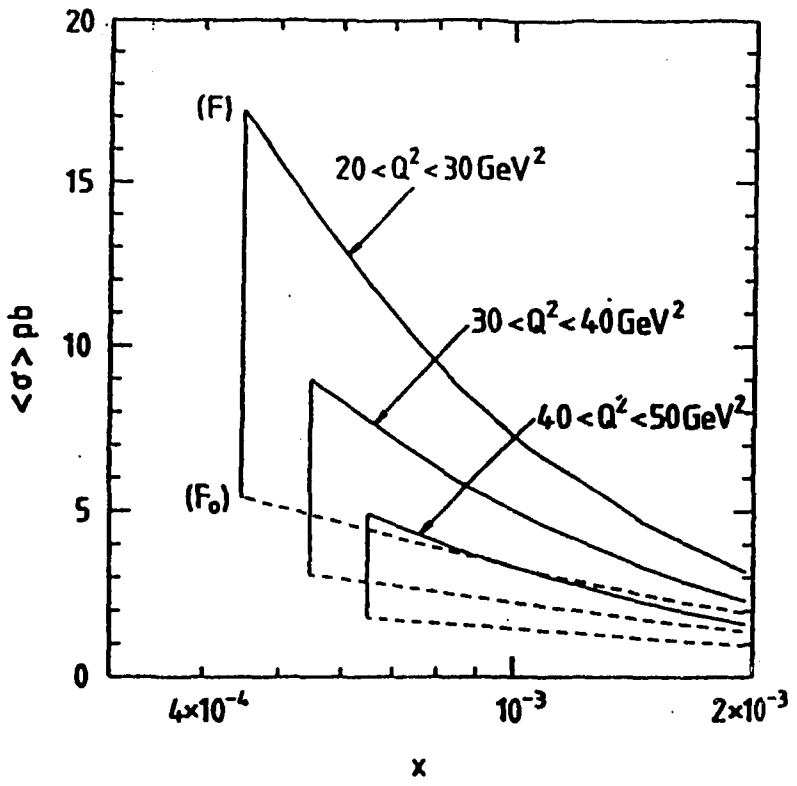
20
15
10
5
0
$\langle\sigma\rangle$ pb
(F)
$20 < Q^2 < 30\,GeV^2$
$30 < Q^2 < 40\,GeV^2$
$40 < Q^2 < 50\,GeV^2$
(F_o)
4×10^{-4}
10^{-3}
2×10^{-3}
x

Fig.17

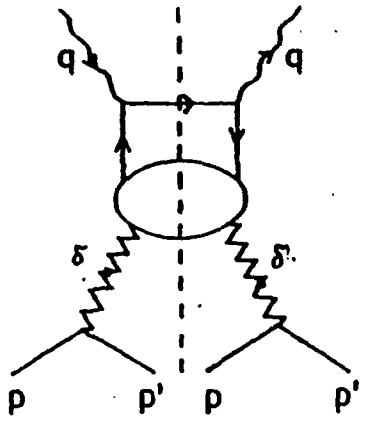

Fig.18

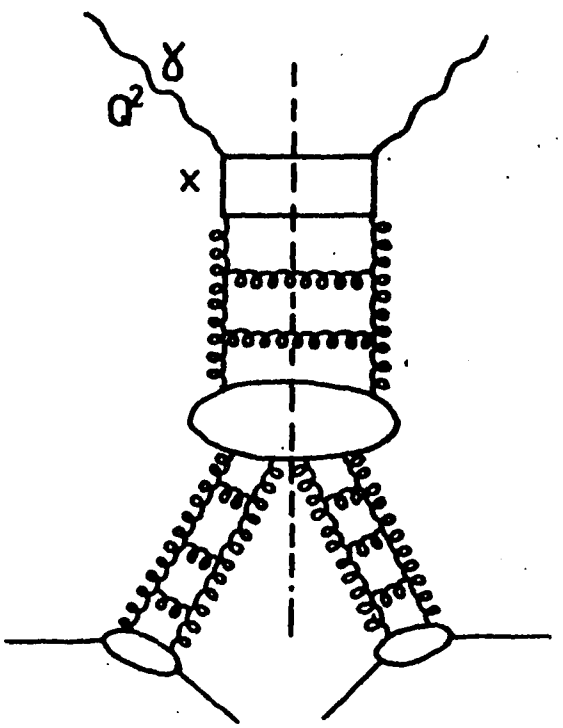

Fig.19

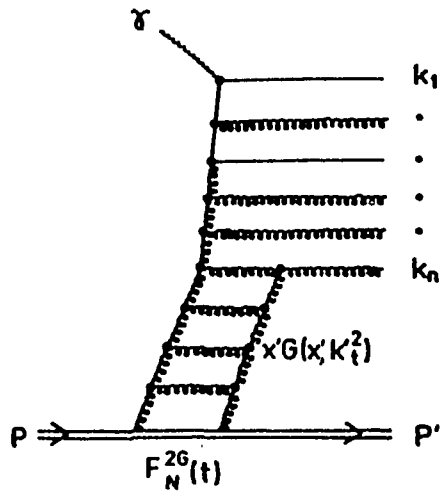
γ
k1
kn
x'G(x',k't²)
P
P'
F2G N(t)

Fig.20

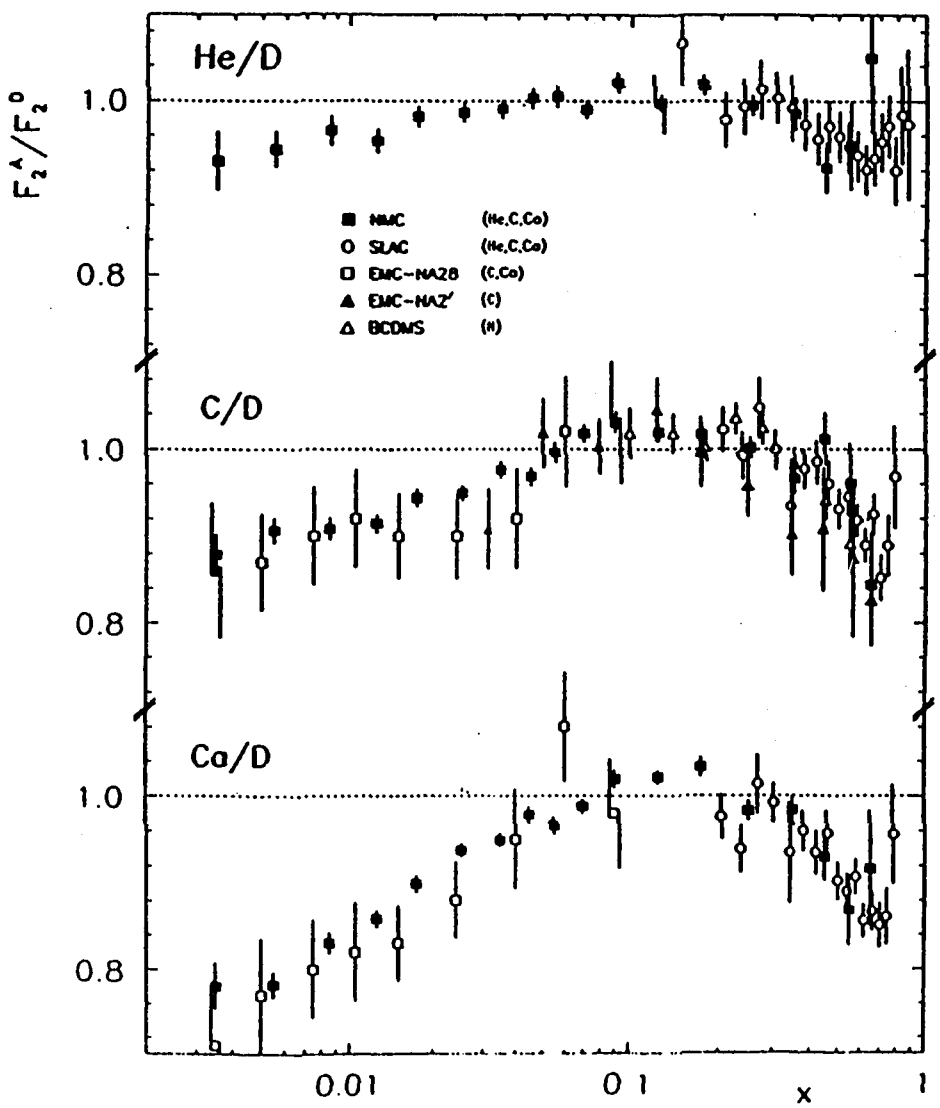
He/D
C/D
Ca/D
F2A/F2D
1.0
0.8
NMC (He,C,Ca)
SLAC (He,C,Ca)
EMC-NA28 (C,Ca)
EMC-NA2' (C)
BCDMS (H)
0.01
0.1
x
1

Fig.21

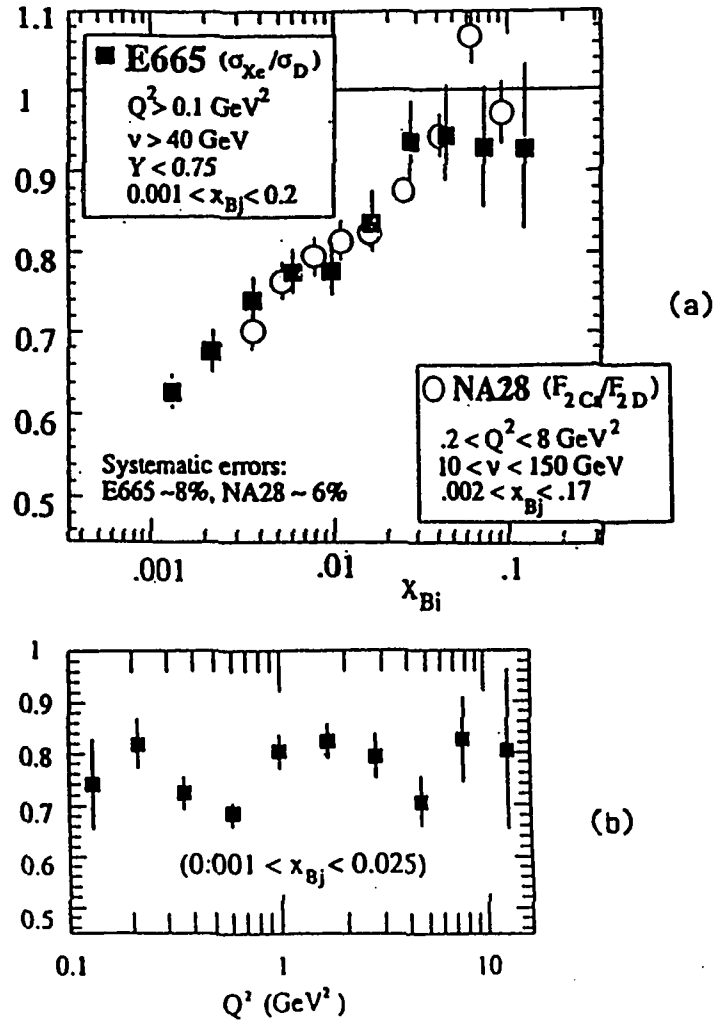
E665 (σ_{Xe}/σ_D)
$Q^2 > 0.1$ GeV^2
$\nu > 40$ GeV
$Y < 0.75$
$0.001 < x_{Bj} < 0.2$
NA28 (F_{2C}/F_{2D})
$.2 < Q^2 < 8$ GeV^2
$10 < \nu < 150$ GeV
$.002 < x_{Bj} < .17$
Systematic errors:
E665 ~8%, NA28 ~ 6%
x_{Bi}
(a)
(0:001 < x_{Bj} < 0.025)
Q^2 (GeV^2)
(b)

Fig.22

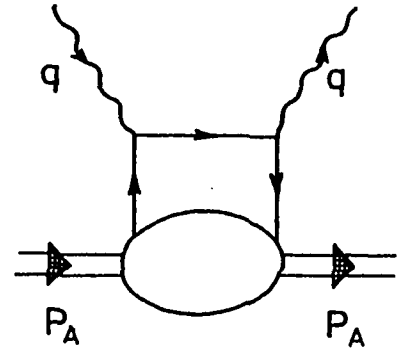
q
q
P_A
P_A

Fig.23

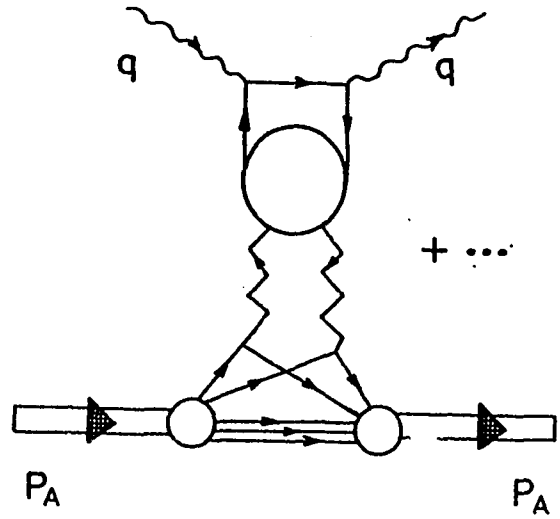

Fig.24

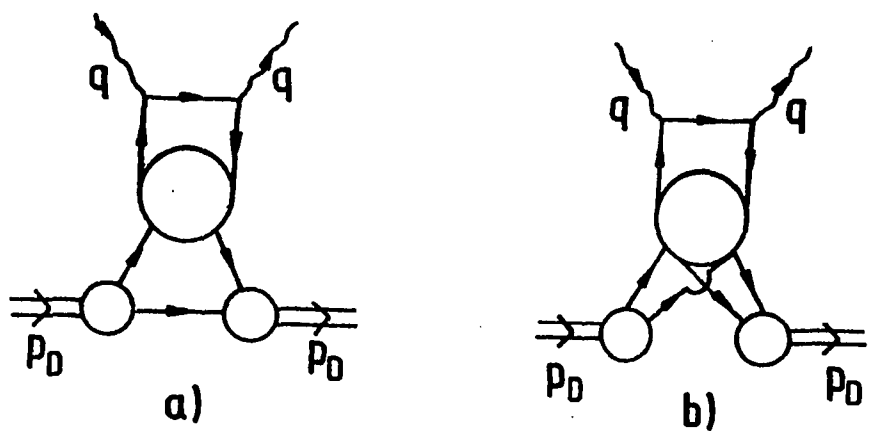

Fig.25

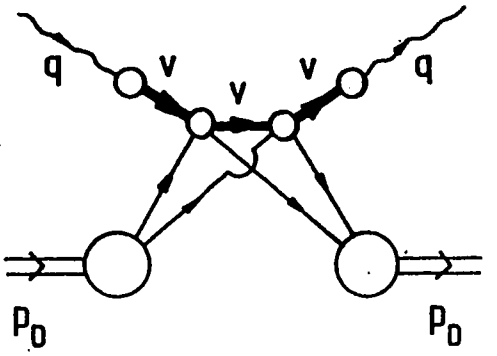
q
V
V
V
q
p_D
p_D

Fig.26

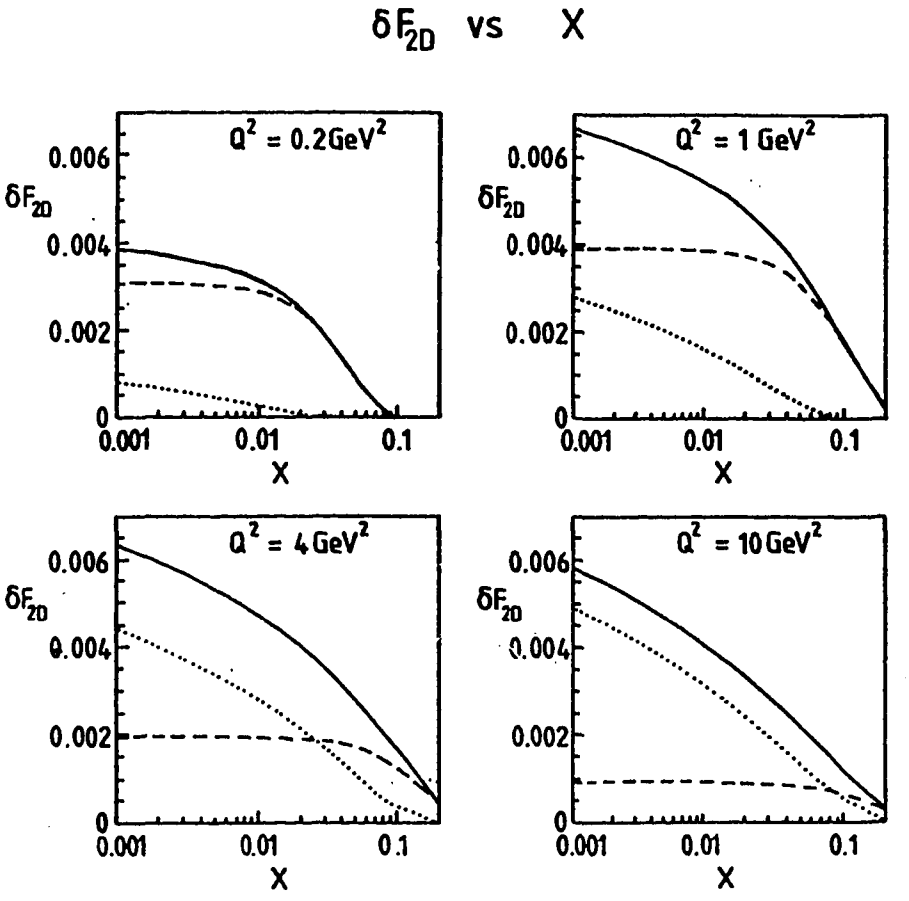
δF_{2D} vs X
$Q^2 = 0.2\,GeV^2$
$Q^2 = 1\,GeV^2$
$Q^2 = 4\,GeV^2$
$Q^2 = 10\,GeV^2$
δF_{2D}
0.006
0.004
0.002
0
0.001
0.01
0.1
X

Fig.27

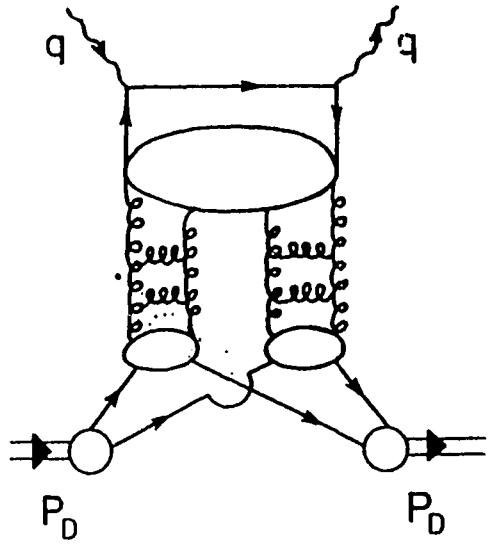
q
q
P_D
P_D

Fig.28

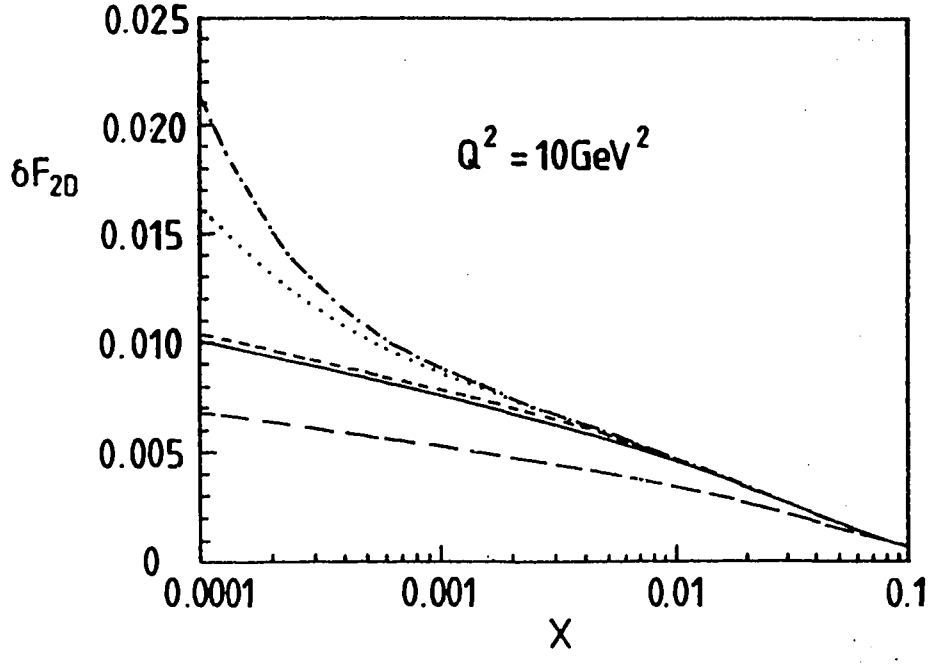
0.025
0.020
0.015
0.010
0.005
0
δF_{2D}
$Q^2 = 10GeV^2$
0.0001
0.001
0.01
0.1
X

Fig.29